https://doi.org/10.5194/amt-2022-51
Preprint. Discussion started: 17 February 2022

Atmospheric Measurement Techniques Discussions

Highly resolved mapping of NO_2 vertical column densities from GeoTASO measurements over a megacity and industrial area during the KORUS-AQ campaign

Gyo-Hwang Choo[1], Kyunghwa Lee[1], Hyunkee Hong[1*], Ukkyo Jeong[2,3], Wonei Choi[4], Scott J. Janz[3]

[1]Environmental Satellite Center, National Institute of Environmental Research, Hwangyeong-ro 42, Seo-gu, Incheon, Republic of Korea, 22689
[2]Earth System Science Interdisciplinary Center, University of Maryland, College Park, Maryland, USA 20740
[3]NASA Goddard Space Flight Center, Greenbelt, Maryland, USA, 20771
[4]Division of Earth Environmental System Science, Major of Spatial Information Engineering, Pukyong National University, Busan 48513, South Korea

Correspondence to: Hyunkee Hong; Tel: +82 32 560 8437; Fax: +82 32 560 8460; E-mail address: wanju77@korea.kr

Abstract. The Korea-United States Air Quality (KORUS-AQ) campaign is a joint study between the United States National Aeronautics and Space Administration (NASA) and the South Korea National Institute of Environmental Research (NIER) to monitor megacity and transboundary air pollution around the Korean Peninsula using airborne and ground-based measurements. Here, tropospheric nitrogen dioxide (NO_2) slant column density (SCD) measurements were retrieved from Geostationary Trace and Aerosol Sensor Optimization (GeoTASO) L1B data during the KORUS-AQ campaign (May 1 to June 10, 2016). The retrieved SCDs were converted to tropospheric vertical column densities using the air mass factor (AMF) obtained from a radiative transfer calculation with trace gas profiles and aerosol property inputs simulated with the Community Multiscale Air Quality (CMAQ) model and surface reflectance data obtained from the Moderate Resolution Imaging Spectroradiometer (MODIS). For the first time, we examine highly resolved (250 m × 250 m resolution) tropospheric NO_2 over the Seoul and Busan metropolitan regions, and the industrial regions of Anmyeon. We reveal that the maximum NO_2 VCDs were 4.94×10^{16} and 1.46×10^{17} molecules cm^{-2} at 9 AM and 3 PM over Seoul, respectively, 6.86×10^{16} and 4.89×10^{16} molecules cm^{-2} in the morning and afternoon over Busan, respectively, and 1.64×10^{16} molecules cm^{-2} over Anmyeon. The data retrieved from the GeoTASO airborne instrument were well correlated with those obtained from the Ozone Monitoring Instrument (OMI) (r = 0.65), NASA's Pandora Spectrometer System (r = 0.84), and NO_2 mixing ratios obtained from in situ measurements (r = 0.78 in the afternoon). Based on our results, GeoTASO is useful for identifying hotspots of NO_2 and its spatial distribution in highly populated cities and industrial areas.

1 Introduction

Nitrogen dioxide (NO_2) is one of the most important atmospheric trace gases and plays a key role in aerosol production and tropospheric ozone photochemistry (Boersma et al., 2004; Richter et al., 2005). Furthermore, high NO_2 concentrations in the

https://doi.org/10.5194/amt-2022-51
Preprint. Discussion started: 17 February 2022

atmosphere have adverse effects on human health, such as respiratory infections and associated symptoms (Brauer et al., 2002; Latza et al., 2009).

The major sources of NO_2 in the atmosphere are from fossil fuel combustion from vehicles and thermal power plants, lightning, flash production, and biogenic soil processes. In addition, it has been found that NO_2 concentrations are highly correlated with population size (Lamsal et al., 2013). The implementation of emission control technology and environmental regulation has led to a decrease in surface NO_2 concentrations in Western Europe, the United States, and Japan in the last few decades (Richter et al., 2005). The NO_2 concentration over major metropolitan cities in South Korea and China are over 3 times larger than over similarly size cites in Europe and United States, despite NO_2 concentration decreasing in China and South Korea (de Foy et al., 2016, Choo et al., 2020).

To date, several low-orbit space borne sensors, such as the Global Ozone Monitoring Experiment (GOME) (Burrows et al., 1999), the Scanning Imaging Spectrometer for Atmospheric Cartography (SCIAMACHY) (Burrows et al., 1995), the Ozone Monitoring Instrument (OMI) (Levelt et al., 2006), the GOME-2 (Callies et al., 2000), and the Tropospheric Monitoring Instrument (TROPOMI) (Veefkind et al., 2012), have monitored atmospheric ozone and its precursors including NO_2 and formaldehyde (HCHO) as a proxy for volatile organic compounds (VOCs). Furthermore, the Geostationary Environment Monitoring Spectrometer (GEMS) (Choi et al., 2018; Kim et al., 2020), which was launched on February 18, 2020 (UTC), will form a constellation of geostationary satellites including the upcoming Tropospheric Emission: Monitoring of Pollution (TEMPO) (Zoogman et al., 2017) and Sentinel-4 platforms, to continuously observe the air quality of the Northern Hemisphere during the daytime.

NO_2 retrievals from space borne hyperspectral measurements are typically conducted using the differential optical absorption spectroscopy (DOAS) method (Platt and Stutz, 2008) to first retrieve the view-dependent slant column density (SCD), and then radiative transfer models are used to determine the vertical column density (VCD) using an air mass factor (AMF) correction. Previous and ongoing space borne instruments use various radiative transfer codes and model input assumptions to calculate NO_2 AMF values at fairly coarse spatial resolution. Since the early 2000s, these include GOME (Richter and Burrows, 2002; Beirle et al., 2003), SCIAMACHY (Sioris et al., 2004), OMI (Boersma et al., 2007), GOME-2 (Richter et al., 2011; Valks et al., 2011), and TROPOMI (Geffen et al., 2020). Because the AMF weighting has a large impact on NO_2 retrievals using the DOAS method, it is important to use model input assumptions that most accurately match the viewing and atmospheric conditions. Several studies have demonstrated the sensitivity of AMF calculations to inaccurate model input parameters (e.g., *a priori* NO_2 vertical profile and aerosol properties) and *a priori* data (cloud information and surface reflectance) (Leitão et al., 2010; Hong et al., 2017; Lorente et al., 2017; Boersma et al., 2018). NO_2 retrievals have also been consistently conducted based on surface remote sensing measurements including the Multi-Axis DOAS (MAX-DOAS), Système D'Analyse par Observations Zènithales (SAOZ) spectrometer (Pastel et al., 2014), and Pandora (Herman et al., 2009) systems. These ground-based measurements can be used as validation references for both airborne and space borne measurements.

https://doi.org/10.5194/amt-2022-51
Preprint. Discussion started: 17 February 2022

Furthermore, NO_2 retrievals from airborne remote sensing instruments, such as the Geostationary Coast and Air Pollution Event (GEO-CAPE) Airborne Simulator (GCAS) (Kowalewski and Janz, 2014), the Geostationary Trace gas and Aerosol Sensor Optimization (GeoTASO) (Leitch et al., 2014), the Airborne Prism Experiment (APEX; Popp et al., 2012), the Airborne Imaging DOAS instrument for Measurements of Atmospheric Pollution (AirMAP; Meier et al., 2017; Schönhardt et al., 2015), the Small Whiskbroom Imager for atmospheric compositioN monitorinG (SWING; Merlaud et al. 2018), and the Spectrolite Breadboard Instrument (SBI; Vlemmix et al., 2017; Tack et al., 2019) have also been performed to identify local emissions sources and obtain highly resolved horizontal NO_2 distributions.

Observations using airborne measurements have an advantage as they enable the observation of horizontal distributions of trace gases at resolutions higher than space-based satellites and provide data over a wider area than ground-based observations. For example, Nowlan et al. (2018) retrieved tropospheric NO_2 VCDs over Houston, Texas, during the Deriving Information on Surface Conditions from Column and Vertically Resolved Observations Relevant to Air Quality (DISCOVER-AQ) campaign and identified a high correlation with data retrieved from Pandora. Popp et al. (2012) also presented the morning and afternoon NO_2 spatial distribution in Zurich, Switzerland, using APEX. Tack et al. (2017) have conducted high-resolution mapping of NO_2 over three Belgium cities (Antwerp, Brussels, and Liège) using APEX and Judd et al. (2020) and Tack et al. (2021) compared NO_2 VCDs retrieved from GCAS/GeoTASO and APEX with those obtained from TROPOMI over New York City and Antwerp and Brussels, respectively. Merlaud et al. (2013) observed NO_2 VCDs over Antwerp using SWING mounted on an unmanned aerial vehicle (UAV). These existing NO_2 retrievals, using airborne measurements, have been useful for constraining regional radiative transfer models due to the highly resolved source identification and the ability to tie these results to the ground-based observations.

This work focuses on airborne NO_2 retrievals from GeoTASO. This instrument was developed by Ball Aerospace to reduce mission risk for the UV-VIS air quality measurements from geostationary orbit for the GEMS and TEMPO missions (Leitch et al., 2014). The retrieval of NO_2, SO_2, and HCHO observed from GeoTASO L1B data using DOAS and principal component analysis (PCA) (Wold et al., 1987) was conducted through the DISCOVER-AQ and KORea-United States Air Quality (KORUS-AQ) campaign (Nowlan et al., 2016; Judd et al., 2018; Choi et al., 2020; Chong et al., 2020). The KORUS-AQ campaign is a joint study between the National Institute of Environmental Research (NIER) and National Aeronautics and Space Administration (NASA) to monitor megacity air pollution and transboundary pollution, and to prepare for geostationary satellite (i.e., GEMS, TEMPO, and Sentinel-4) air quality observability (of trace gases and aerosols) from May to June 2016.

Although surface NO_2 concentrations in South Korea are high due to high population density, high traffic volumes, and many industrial complexes and thermal power plants, and whereas NO_2 retrieval studies using airborne and ground measurements over North America, Europe, China, and Japan have been conducted, data for South Korea remain limited.

In this study, NO_2 VCD retrieval was conducted using solar backscattered radiance observed from GeoTASO over South Korea during the KORUS-AQ campaign. The specific aims of this study are as follows:

(1) To retrieve tropospheric NO_2 vertical column data using GeoTASO measurements over polluted regions of the Seoul and Busan metropolitan areas and the Anmyeon industrial regions of the Korean Peninsula.

(2) To estimate NO_2 VCD uncertainties using error propagation accounting for spectral fitting errors and AMF uncertainties associated with input data errors, including aerosol optical depth (AOD), single scattering albedo (SSA), aerosol loading height (ALH), and surface reflectance.

(3) To compare NO_2 VCDs retrieved from GeoTASO and those obtained from OMI and ground-based Pandora instruments, as well as surface in situ measurements.

2 KORUS-AQ campaign area, measurements, and model simulation

2.1 Campaign area

As shown in Fig. 1, GeoTASO observations were conducted focusing on highly NO_2-polluted regions in the Seoul and Busan metropolitan areas and the Anmyeon during the KORUS-AQ campaign. The Seoul metropolitan area (Seoul Special City, Gyeonggi Province, and Incheon City) is one of the most densely populated areas worldwide, with a population of approximately 20 million in 2016. Busan is the second-largest city in South Korea, with a population of approximately 3.4 million in 2016. Anmyeon is located southwest of Seoul with petrochemical complexes, steel mill works, and thermal power stations in this area. The background colour in Fig. 1 represents the average NO_2 VCD obtained from the OMI during the KORUS-AQ campaign period, showing over 1×10^{16} molecules cm^{-2} over the Seoul metropolitan area. The average tropospheric NO_2 VCD data were excluded from 30 May 2016 to 9 Jun 2016, when the OMI L2 data did not exist during the campaign period.

2.2 Pandora

NO_2 VCDs retrieved from the GeoTASO were validated using those from NASA's Pandora Spectrometer system. The Pandora spectrometer is a hyper-spectrometer that can provide direct sun measurements of UV/Vis spectra (280–525 nm with a full width at half maximum (FWHM) of 0.6) for observing atmospheric trace gases. During the KORUS-AQ, eight Pandora instruments monitored NO_2 and ozone (O3) VCD as depicted as plus symbols in Fig. 1. The retrieved data are available on the KORUS-AQ pages of NASA's Goddard Space Flight Center website (https://avdc.gsfc.nasa.gov/pub/DSCOVR/Pandora/DATA/KORUS-AQ/). We compared NO_2 VCDs obtained from Pandora within 1 km and 30 min with those from GeoTASO. Because NO_2 has a short atmospheric lifetime, especially during the summer (Shah et al., 2020), its spatial and temporal distributions vary notably A detailed description of Pandora's operation during the KORUS-AQ campaign has been previously reported (Herman et al., 2018; Spinei et al., 2018).

2.3 Ground-based in situ NO_2 measurement

Although the physical units of VCD and surface mixing ratio from in-situ measurements are different, comparison of their spatiotemporal variations provides useful information for deriving surface air quality from airborne instruments (e.g., Jeong

https://doi.org/10.5194/amt-2022-51
Preprint. Discussion started: 17 February 2022

and Hong, 2021a; 2021b *and references therein*). In this study, we compared the NO_2 VCDs (molecules cm^{-2}) retrieved from GeoTASO to surface mixing ratios measured by ground-based in-situ monitoring network over South Korea (i.e., Air-Korea, a national real-time air quality network; https://www.airkorea.or.kr/). The instruments utilize the chemiluminescence method (Kley and McFarland, 1980), and approximately 400 air quality monitoring sites in Korea are registered in the system, providing hourly surface NO_2 concentrations. We compared NO_2 VCDs retrieved from GeoTASO within 0.5 km and 30 min with NO_2 concentrations obtained from Air-Korea

2.4 GeoTASO measurement

NO_2 VCDs were retrieved from the L1B radiance dataset (version: V02y) obtained using GeoTASO during the KORUS-AQ campaign. The NASA Goddard Space Flight Center conducted the L1B radiance calibration, which included offset and smear collection, gain matching, amplifier cross-talk correction, dark rate correction, integration normalisation, sensitivity derivation, wavelength registration, geo-registration, non-linearity correction, and ground pixel geolocation (Kowalewski et al., 2017; Chong et al., 2020). The detailed specifications of GeoTASO are listed in Table 1. During the KORUS-AQ campaign, measurements of air pollutants were made using the GeoTASO on board the NASA Langley Research Center B200 aircraft to monitor air quality and long-range transport of pollutants over the Korean Peninsula. In total, 30 observations were conducted between 29 April and 10 June 2016. Most observations were made once or twice a day, Fig. 1 shows the flight routes of B200 and the tropospheric NO_2 VCDs obtained from the OMI during the campaign period. The observations were concentrated in the metropolitan areas of Seoul and Busan and the industrial areas of Anmyeon, with a flight altitude of 8,000–9,000 m. Fig. 2 shows the flowchart for retrieving the tropospheric NO_2 VCD from the GeoTASO.

2.4.1 NO_2 slant column density retrieval

We first retrieved NO_2 SCDs using the DOAS method (Platt, 1994). Nonlinear least square minimisation was used to retrieve the NO_2 SCDs which minimize the difference between the measured optical depth and the modelled value in QDOAS software (Eq. (1); Danckaert et al., 2012).

$$\frac{\ln I(\lambda)}{\ln I_0(\lambda)} = -(\sum_{j=1}^{m} \rho_j \times \sigma'_j(\lambda) + B(\lambda) + R(\lambda) + A(\lambda) + N(\lambda)) \tag{1}$$

Where I(λ) is the measured earthshine radiance at wavelength λ; I_0 is the reference radiance from the sea surface south of Jeju Island (red circle in Fig. 1, 32.983°N, 126.392°E) on 1 May 2016. The Community Multiscale Air Quality (CMAQ) modelling system data indicated that the NO_2 VCD from the surface to 50 hPa at this point on this day was 6.751 × 10^{15} molecules cm-^{2}; ρ_j represents the SCD of each species j; $\sigma'_j(\lambda)$ represents the convoluted gas absorption cross-section with the Gaussian distribution function (GDF) with GeoTASO FWHM (the UV and VIS range were 0.34−0.49 nm and 0.70−1.00 nm, respectively (Nowlan et al., 2016)) at wavelength λ of species j, respectively. The spectral fitting window was selected from 425 to 450 nm. To determine the wavelength registration more accurately in the narrow fitting window, additional wavelength calibration of the spectra for each of the 33 across track pixels was performed using a high-resolution solar reference spectrum

https://doi.org/10.5194/amt-2022-51
Preprint. Discussion started: 17 February 2022

Atmospheric Measurement Techniques Discussions

(Kurucz solar spectrum) (Chance and Kurucz, 2010) with the GDF. The absorption cross-sections of NO_2 (Vandaele et al., 1998), O_3 (Bogumil et al., 2000), H_2O, and the ring effect as pseudo-absorbers (Chance and Spurr, 1997) were used to construct the model equation; and B(λ), R(λ), A(λ), and N(λ) are the broad absorption of the trace gases, extinction by Mie and Rayleigh scattering, variation in the spectral sensitivity of the detector or spectrograph, and noise, respectively, which were accounted by an 8th order polynomial. An example of the spectral fitting results is presented in Fig. 3.

2.4.2 NO_2 AMF calculation

AMF, the ratio of SCD to VCD, can be calculated using the scattering weight (ω) and shape factor (S) (Palmer et al., 2001) in Eq. (2)−(5).

$$\mathrm{AMF} = \frac{SCD}{VCD} \quad (2)$$

$$\mathrm{AMF} = AMF_G \int_{z1}^{z2} \omega(z) S(z)\, dz \quad (3)$$

$$\omega(z) = -\frac{1}{AMF_G}\frac{\partial \ln I_B}{\partial \tau} \quad (4)$$

$$S(z) = \frac{\alpha(z) n(z)}{\int_{z1}^{z2} \alpha(z) n(z)\, dz} \quad (5)$$

Where AMF_G represents the geometric AMF, I_B is the earthshine radiance, τ is the optical depth, α is the absorption cross-section, and n is the number density of the absorber. NO_2 AMF was calculated using a linearised pseudo-spherical scalar and vector discrete ordinate radiative transfer model (VLIDORT, version 2.6; Spurr and Christi, 2014). Aerosol properties, such as AOD, SSA, and *a priori* NO_2 vertical profile information, were simulated using the CMAQ, and surface reflectivity was obtained from the Moderate Resolution Imaging Spectroradiometer (MODIS) (Collection 6). The surface reflectance product, MOD09CMG and MYD09CMG, provide an estimate of the surface spectral reflectance at ground level in the absence of cloud and atmospheric absorption or scattering and are available at a 0.05 degree (~5.6 km) spatial resolution. In previous studies (Lamsal et al., 2017; Nowlan et al., 2018; Judd et al., 2019; Chong et al., 2020), an AMF were described for both above and below aircraft altitude is used to convert NO_2 SCDs to VCDs using Eq. (6)−(8).

$$\mathrm{AMF}\uparrow = AMF_G \int_{Z_A}^{Z_{TOA}} \omega(z) S(z)\, dz \quad (6)$$

$$\mathrm{AMF}\downarrow = AMF_G \int_{Z_0}^{Z_A} \omega(z) S(z)\, dz \quad (7)$$

$$NO_2\ \mathrm{VCD}\downarrow = \frac{NO_2\, SCD - AMF\uparrow \cdot NO_2 VCD\uparrow}{AMF\downarrow} \quad (8)$$

Where $AMF\uparrow$ and $AMF\downarrow$ are AMF above and below aircraft, respectively, and $NO_2\ VCD\uparrow$ represents NO_2 VCD above the aircraft obtained from a chemical transport model (CTM). However, here we calculated NO_2 VCD↓ by dividing NO_2 SCDs by $AMF\downarrow$ because stratospheric NO_2 ($NO_2\ VCD\uparrow$) concentrations are much lower than tropospheric NO_2 concentrations, especially in megacities and industrial areas (Valks et al., 2011).

https://doi.org/10.5194/amt-2022-51
Preprint. Discussion started: 17 February 2022

2.5 Chemical model description

Vertical profiles from CMAQ (Byun and Ching, 1999; Byun and Schere, 2006), a CTM, were used to calculate AMFs. CMAQ simulations were conducted with a horizontal resolution of 15 × 15 km and had 27 vertical layers from the surface to 50 hPa. The meteorological fields were prepared using the advanced research weather research and forecasting (ARW-WRF) model (Skamarock et al., 2008). Anthropogenic emissions were generated based on the KORUS v5.0 model (Woo et al., 2012), and biogenic emissions were simulated using the Model of Emissions of Gases and Aerosols from Nature (MEGAN v2.1; Guenther et al., 2006; 2012). Besides anthropogenic and biogenic emissions, the Fire Inventory from NCAR (FINN; Wiedinmyer et al., 2006, 2011) was utilised to update the pyrogenic emission fields. Details of the model descriptions have been provided by Lee et al. (2020).

3 Results and discussion

3.1 NO_2 VCD retrieval

3.1.1 Seoul metropolitan region

The population of the Seoul metropolitan region is approximately 20 million, which is approximately 40% of the total population of South Korea. It is very rare to obtain high-resolution horizontal NO_2 VCD distributions using airborne measurements in the morning and afternoon, especially in Asian megacities. Fig. 4 shows tropospheric NO_2 VCDs over Seoul on 9 June 2016, at 9 AM and 3 PM local time (LT). According to the Terra/Aqua CLDMASK data (Ackerman et al., 1998), on this day, the cloud fraction was less than 0.3 over the entire domain of Fig. 4.

In the morning, NO_2 VCDs retrieved from GeoTASO were highly correlated with expressways (red boxes in Fig. 4), such as the Gyeongin, Seohaean, and Gyeongbu Expressways, and over major cities with heavy traffic, such as Seoul, Bucheon, Ansan, Anyang, and Suwon. GeoTASO observed NO_2 VCD values three-times higher (>3 × 10^{16} molecules cm^{-2}) in these areas compared to the surrounding rural areas. In particular, high NO_2 VCD values above 6 × 10^{16} molecules cm^{-2} were observed above the Gyeongin Expressway, which has very heavy traffic in a relatively short section, and the Gunpo Complex Logistics zone, where diesel vehicle traffic is also high. The major NO_2 source regions and the regions where high NO_2 VCD values were observed were highly consistent at 9 AM because the wind speed at this time—as obtained from the unified model (UM) based Regional Data Assimilation and Prediction System (RDAPS) of the Korea Meteorological Administration (KMA)—was as low as 0.1 ms^{-1}. The average daily traffic volume of these expressways exceeds 150,000 vehicles, and the total number of vehicles registered in these major cities is > 6,000,000, with an average daily mileage per car of over 38 km. Detailed information on these cities and expressways is listed in Table 2 and Table 3. Based on the level of vehicular traffic, combustion using gasoline and diesel engines leads to high overall emissions of NO_2 in the Seoul metropolitan region (Kendrick et al., 2015).

Compared to the morning, the afternoon had extremely high tropospheric NO_2 VCD values (exceeding 5×10^{16} molecules cm^{-2}) in most of the Seoul metropolitan regions including rural areas, whereas the NO_2 mixing ratio (MR) obtained from Air-Korea decrease in the afternoon. According to Tzortziou et al. (2018), similar results were retrieved from the Pandora site in Seoul, with higher afternoon NO_2 VCDs than in the morning. This result is presumed to be due to the reason that the amount of NO_2 produced by chemical conversion of nitric oxide (NO) by O_3 and VOCs in the atmosphere, along with NOx generated by regional emissions (traffic) in the Seoul metropolitan region, is greater than the amount lost by photolysis and transport to nearby areas (Herman et al., 2018). In addition, the increase in tropospheric NO_2 VCD in the afternoon is presumed to be due to the accumulation and dispersion of NO_2 according to the change in the planetary boundary layer height (Ma et al., 2013).

3.1.2 Industrial and power plant regions in Anmyeon

The high spatial resolution of tropospheric NO_2 VCD from GeoTASO over the Anmyeon industrial region, where many industrial facilities and several power plants are distributed, is shown in Fig. 5. The panels a and b of this figure show tropospheric NO_2 VCD and NO_2 SCD retrieved from GeoTASO L1B data, respectively, between 13:00 and 17:00 LT on 5 June 2016. The panel c depicts the calculated AMF of NO_2 over the domain. The GeoTASO observations clearly detected moderate and strong NO_2 emission sources over this area: (1) Boryeong power plant, (2) the Hyundai integrated steelworks, (3) Dangjin power plant, (4) the Daesan Petrochemical Complex, and (5) Taean power plant. High NO_2 VCD values (> 5×10^{16} molecules cm^{-2}) were observed over steel mill works, petrochemical complexes, and power plants, whereas values were comparatively low (<1×10^{16} molecules cm^{-2}) over small cities including Seosan, Dangjin, and Boryeong with populations of less than 0.1 million, and the Seohaean Expressway. In 2016, the annual NOx emissions by the Hyundai steelworks and the Dangjin and Boryeong power plants were 10,271,075, 11,852,972, and 16,788,438 kg $year^{-1}$, respectively. NO_2 emission rates from major industrial facilities in the Anmyeon region are shown in Table 4. Fig. 5 shows high NO_2 concentrations of major industrial facilities in the Anmyeon region, where fossil fuel combustion in factories and thermal power plants leads to high emissions (Prasad et al., 2012). Due to relatively sparse distribution over rural areas, the Air-Korea measurements did not detect the major NO_2 plume as shown in Fig. 5a. Thus, airborne remote sensing systems, such as GeoTASO, can effectively compliment the ground-based networks for monitoring minor and major NO_2 emissions, particularly over these remote industrial regions.

The GeoTASO data captured not only NO_2 emissions from the chimneys of steelworks and power plants but also its transport by the wind. Fig. 6a and 6b show enlarged views of tropospheric NO_2 SCD retrieved using GeoTASO over the Hyundai steelworks (red box in Fig. 5) and the Boryeong power plant (white box in Fig. 5). The arrows in Fig. 6 represent the prevailing wind direction and speed from RDAPS. NO_2 emitted from the chimneys of these sites was transported to the Yellow Sea, travelling distances of over 26 km at speeds of approximately 6 ms-1. According to Chong et al. (2020), similar results were found for SO_2 emitted and transported from these sites.

https://doi.org/10.5194/amt-2022-51
Preprint. Discussion started: 17 February 2022

Atmospheric Measurement Techniques Discussions

3.1.3 Busan metropolitan region

Fig. 7a and 7b show tropospheric NO_2 VCD retrieved from the GeoTASO L1B data over the Busan metropolitan region on 10 June 2016 in the morning (between 08:00 and 11:00 LT) and afternoon (between 13:00 and 16:00 LT), respectively. High NO_2 VCDs were observed above urban areas, the port, industrial complexes, and the inter-city road between Busan and Changwon. Similar to the Seoul metropolitan regions, it is estimated that combustion using gasoline and diesel engines contributes to the high NO_2 emission. In the morning, NO_2 VCDs were high (approximately 3×10^{16} molecules cm^{-2}) in the major cities and, especially, around Busan Newport, with values exceeding 7×10^{16} molecules cm^{-2}. In comparison, in the mountainous regions between Daegu and Busan, NO_2 VCD values were less than 1×10^{16} molecules cm^{-2} during the same period. The spatial distribution of tropospheric NO_2 VCDs was similar to that in the Seoul metropolitan regions, which high values over major cities and roads (compare Fig. 4 and 7). In Busan, fossil fuel combustion using both road vehicles and ships likely contributes to the NO_2 emissions. In the afternoon, unlike Seoul metropolitan region, tropospheric NO_2 VCD over Busan decreased by over 3×10^{16} molecules cm^{-2}, which also corresponds with NO_2 MR data obtained from the Air-Korea sites. Detailed information on these cities is listed in Table 5.

3.2 Error estimation

NO_2 VCD retrieval accuracy using the DOAS method depends on both the AMF calculation and spectral fitting error of SCD retrieval. Retrieval errors of the NO_2 VCD were estimated using error propagation analysis as expressed in Eq. (9).

$$\frac{\varepsilon_{VCD}}{VCD} = \sqrt{(\frac{\varepsilon_{SCD}}{SCD})^2 + (\frac{\varepsilon_{AMF}}{AMF})^2} \quad (9)$$

Where ε_{VCD} is the total error of NO_2 VCD. The error of NO_2 SCD (ε_{SCD}) is obtained from the spectral fitting error of NO_2 SCD via DOAS spectral fitting. ε_{AMF} indicates the error of NO_2 AMF caused by uncertainties in the model input parameters for AMF calculation. Uncertainties in aerosol properties (AOD, SSA, and ALH) and surface reflectance for the RTM calculations are known to be the major factors affecting NO_2 AMF accuracy (Boersma et al. 2004; Leitão et al., 2010; Hong et al., 2017). Therefore, in this present study, we quantified the NO_2 AMF errors (ε_{AMF}) due to uncertainties in the input parameters independent of one another using Eq. (10):

$$\varepsilon_{AMF} = \sqrt{(\frac{\partial AMF}{\partial AOD})^2 \sigma AOD^2 + (\frac{\partial AMF}{\partial SSA})^2 \sigma SSA^2 + (\frac{\partial AMF}{\partial ALH})^2 \sigma ALH^2 + (\frac{\partial AMF}{\partial SFR})^2 \sigma SFR^2} = \sqrt{\sum_{i=1}^{4} (\frac{\partial AMF}{\partial \chi_i})^2 \sigma_{\chi_i}^2}, \quad (10)$$

where $\frac{\partial AMF}{\partial \chi_i}$ are partial derivatives of NO_2 AMF with respect to the input parameters (χ_i), $\sigma_{\chi i}$ represents the uncertainty of the χ_i. The σ of AOD, SSA, ALH, and surface reflectance are assumed as 20%, 4%, 20%, and 20%, respectively, in this study. To derive $(\frac{\partial AMF}{\partial \chi_i})^2$, the true χ_i is input to the RTM to simulate 'true' NO_2 AMF. For the AOD, SSA, ALH, and surface reflectance (SFR), perturbed NO_2 AMF was simulated using RTM with $\chi_i + \sigma\chi_i$. $\partial\chi_i$ denotes the difference between the 'true' χ_i and $\chi_i + \sigma\chi_i$, and ∂AMF is the difference between the 'true' NO_2 AMF simulated with 'true' input values and the new NO_2 AMF simulated using input parameters, with the uncertainty of each parameter being $\chi_i + \sigma\chi_i$. The simulation for calculating the

ε_{AMF} was conducted using the input parameters on 9 June 2016. The error estimation was conducted for the pixels where root mean square residual < 0.001 and NO_2 VCD > 5 × 10^{15} molecules cm^{-2} since NO_2 SCD precision is reported to be highly decreased in low NO_2 conditions (Hong et al., 2017).

Table 6 lists the estimated NO_2 VCD error for each sources based on the error propagation method. The total NO_2 VCD error was 14.3% with a high portion of NO_2 SCD error (11.9%), showing the importance of accurate DOAS spectral fitting to derive NO_2 SCD. The total AMF error due to uncertainties in input parameters was calculated to be 7.3%. Among model input parameters, the uncertainties in SFR and SSA had the greater effect on the NO_2 AMF calculation error (5.2% and 4.1%, respectively) than those in other input parameters. The NO_2 AMF errors due to uncertainties in AOD and ALH are estimated to be 2.0% and 1.0%, respectively. Nevertheless, ALH sensitively affects NO_2 AMF because near the surface where trace gases and aerosols are well mixed, aerosols lead to multiple scattering effects and the light absorption of trace gases due to increasing light path (Castellanos et al., 2015; Hong et al., 2017). The accuracy of ALH is important to calculate AMF, especially in the Asia region where high loadings of aerosol plumes persists throughout the year.

In this present study, we additionally investigated the spatial distribution of AMF calculation errors associated with uncertainties in aerosol properties (AOD, SSA, ALH, and SFR). Fig. 8a and 8b show the percent difference error between the calculated AMFs using the CMAQ AOD data with 20% lower (Fig. 8a) and 20% higher (Fig. 8b) values, respectively. The AMF decreased and increase by up to 5% with decreasing and increasing AOD, respectively, in the Seoul metropolitan region. We estimated that, under low aerosol loading conditions, an increase in AOD near the surface leads to an increase in the scattering probability within the surface layer with high NO_2 concentrations.

Fig. 8c shows the percent difference error between the calculated AMFs using CMAQ SSA data with a 0.04 lower value. The AMF decreased with decreasing SSA because the absorption of light increased. The ALH was also found to affect the accuracy of the AMF calculations. On 9 June 2016, the average ALH over Seoul was just 0.27 km, meaning that a 20% change in ALH equates to approximately 50 m. Nevertheless, the AMF is sensitive to the ALH near the surface as trace gases and aerosols are mixed in this layer, and aerosols lead to multiple scattering effects, and the light absorption of trace gases also occurs due to increased light paths (Castellanos et al., 2015; Hong et al., 2017). The accuracy of ALH is, therefore, important for calculating AMF.

Fig. 8f and 8g show the percent difference error between the calculated AMFs using the MODIS surface reflectance data with 20% lower (Fig. 8f) and 20% higher (Fig. 8g) values, respectively. The AMF decreased by about 8% when surface reflectance decrease, and vice versa when it increased.

3.3 Validation of NO_2 VCDs retrieved from GeoTASO

Tropospheric NO_2 VCDs retrieved from GeoTASO L1B data ($NO_{2,G}$) were compared with those obtained from Pandora ($NO_{2,P}$), and NO_2 MRs ($NO_{2,A}$) observed from surface in situ instruments at Air-Korea sites. The OMI NO_2 VCDs ($NO_{2,O}$) were only available for 10 June during the campaign period. Therefore, we only compared 53 $NO_{2,G}$ and $NO_{2,O}$ data points within a radius of 25 km and 30 min, which yielded a correlation coefficient of 0.65 with a slope of 0.43..

https://doi.org/10.5194/amt-2022-51
Preprint. Discussion started: 17 February 2022

3.3.1 Comparing NO_2 VCD from GeoTASO to Surface NO_2 mixing ratios

To evaluate the spatiotemporal distribution of NO_2 VCDs retrieved from GeoTASO, $NO_{2,G}$ in comparisons to surface spatial patterns, $NO_{2,G}$ was compared with $NO_{2,A}$ for GeoTASO data within a radius of approximately 0.5 km and 30 min (Fig. 9). The correlation coefficient (R) between $NO_{2,G}$ (molecules cm-^{2}) and $NO_{2,A}$ (ppmv) at 9 AM and 3 PM LT in the Seoul metropolitan region was 0.38 and 0.78, respectively. When using only roadside station data from Air-Korea, the R-value for the morning increased to 0.83, which implies GeoTASO is more sensitive to emissions from NO_2 source areas, such as roadsides.

In the Busan metropolitan area, the R-value of the $NO_{2,G}$ and $NO_{2,A}$ data had a correlation coefficient greater than 0.67. This reflects the more even horizontal distribution of NO_2 in the afternoon, when diffusion from the source areas had taken place. However, for a more accurate comparison, NO_2 VCD data should be converted to NO_2 MR based on mixing layer height, temperature, and pressure profile data (Kim et al., 2017; Qin et al., 2017; Jeong and Hong, 2021a).

3.3.2 Comparing NO_2 from GeoTASO and Pandora systems

To validate the accuracy of $NO_{2,G}$ data, we made a comparison with NO_2 VCD obtained from the Pandora system ($NO_{2,P}$) during the KORUS-AQ campaign period. $NO_{2,P}$ obtained from Busan University, Olympic Park, Songchon, Yeoju, and Yonsei University Pandora sites on June 5, 9, and 10 were used for the GeoTASO validation (Fig. 1). $NO_{2,G}$ and $NO_{2,P}$ columns at these sites are compared in Fig. 10. The $NO_{2,G}$ data available within 30 min from each Pandora measurement time were compared with $NO_{2,P}$. When the radius distance of the observation locations was less than approximately 1 km (black circles in Fig. 10), $NO_{2,G}$ and $NO_{2,P}$ were strongly correlated (R = 0.94, with a slope of 1.48). This is considered because of the difference of light paths between GeoTASO in nadir viewing mode and Pandora in direct sun mode, particularly when they take measurements in a large city with high vertical and horizontal NO_2 variations.

The correlation was lower with an increase in distance between the Pandora and GeoTASO observation locations; the correlation decreased to 0.84 when the radius distance was <5 km. This indicates the impact of the spatial gradient of NO_2 within that radius not captured using Pandora's local observation. When $NO_{2,P}$ was lower than 1×10^{16} molecules cm^{-2}, the correlation coefficient between $NO_{2,G}$ and $NO_{2,P}$ at both 1 km and 5 km distances was <0.1. The weak correlation at low NO_2 levels most likely reflects the differences in viewing geometries and the horizontal inhomogeneity of the measured NO_2 between Pandora and GeoTASO.

4. Conclusions

For the first time, we have retrieved NO_2 VCD data using airborne GeoTASO observations over the Seoul metropolitan region—one of the most populous cities worldwide, the Busan metropolitan region—the second-largest city in South Korea, and Anmyeon, with thermal power plants and industrial complexes. By retrieving NO_2 data using GeoTASO L1B radiance, it

https://doi.org/10.5194/amt-2022-51
Preprint. Discussion started: 17 February 2022

was possible to observe the spatial distribution of NO_2 over these metropolitan and industrial regions. In the morning, tropospheric NO_2 VCD over Seoul showed a strong horizontal gradient between rural and urban areas. In urban areas, tropospheric NO_2 VCD was high, with values exceeding 3×10^{16} molecules cm^{-2}; in rural areas, values were typically below 1×10^{16} molecules cm^{-2}. Extremely high values over 10×10^{16} molecules cm^{-2} were also observed in both rural and urban areas. In Anmyeon, GeoTASO observations showed NO_2 is mainly emitted from the chimneys of industrial complexes and thermal power plants, and subsequently transported by wind approximately 30 km to the Yellow Sea of the west coast of the Korean Peninsula. In the Busan metropolitan region, in the morning, tropospheric NO_2 VCDs showed a similar pattern to the Seoul metropolitan region, with high values above the inter-city road. However, in contrast to Seoul, tropospheric NO_2 VCDs in Busan decreased in the afternoon.

To validate the data retrieved from the GeoTASO system, we compared $NO_{2,G}$ with $NO_{2,O}$ obtained from the OMI, $NO_{2,A}$ obtained from Air-Korea, and $NO_{2,P}$ obtained from the Pandora observation system. When the distance between two observations was approximately 25, 0.5, or 1 km within 30 min, the correlation coefficients were relatively high ($R = 0.65$, 0.67, and 0.84, respectively). However, the correlation between $NO_{2,G}$ and $NO_{2,A}$ over the Seoul metropolitan region was weak ($R = 0.38$) in the morning because of the more pronounced NO_2 horizontal gradient.

The GeoTASO system successfully observed NO_2 VCDs with a high horizontal spatial resolution for both metropolitan and industrial regions. This demonstrates that airborne remote sensing measurements, such as those obtained from GeoTASO, GCAS, and APEX, can be a very effective tool for the validation of trace gases retrieved from environmental satellites, including the OMI, TROPOMI, and GOME-2; these systems can obtain high-resolution measurements over relatively wide areas. However, to validate geostationary environmental satellites with higher spatiotemporal resolutions, such as the GEMS, TEMPO, and sentinel-4, additional validation strategies are needed. First, based on error estimation, aerosol properties should be determined and NO_2 vertical profile retrieval performed using, for example, LIDAR, MAX-DOAS, and sondes. This is important because the accuracy of aerosol properties and the NO_2 vertical profiles affect the accuracy of AMF calculations (Leitão et al., 2010; Hong et al., 2017; Lorente et al., 2017; Boersma et al., 2018). Furthermore, as we observed in the Seoul metropolitan area, more closely spaced observations using ground-based remote sensing systems and in situ measurements are needed as NO_2 displays large horizontal gradients, especially in the morning.

Author contributions

GH and **HH** designed and implemented the research. **KL** provided the CTM data. **GH** developed the code for model running and performed the RTM simulations. **HH** and **UJ** contributed to the analysis of ground-based data. **GH** and **WC** carried out the sensitivity test. **GH**, **KL**, **HH**, **UJ**, **WC,** and **JJS** revised and edited the paper. **HH** and **UJ** provided constructive comments. All authors contributed to this works.

Competing interests

The authors declare that they have no conflict of interest.

Acknowledgements

Pandora data were obtained from the KORUS-AQ home pages of NASA's Goddard Space Flight Center (https://avdc.gsfc.nasa.gov/pub/DSCOVR/Pandora/DATA/KORUS-AQ/). Ground-based NO_2 MR data were obtained from Air-Korea (http://www.airkorea.or.kr/web/detailViewDown?pMENU_NO=125/). The authors would like to thank KORUS-AQ campaign team for providing the GeoTASO and Pandora data.

Funding

This work was funded by the National Institute of Environmental Research (NIER) of Ministry of Environment [No. NIER-2021-01-01-100].

References

Ackerman, S. A., Strabala, K. I., Menzel, W. P., Frey, R. A., Moeller, C. C., and Gumley, L. E.: Discriminating clear sky from clouds with MODIS, J. Geophys. Res., 103, 32141–32157, https://doi.org/10.1029/1998JD200032, 1998.

Beirle, S., Platt, U., Wenig, M., and Wagner, T.: Weekly cycle of NO_2 by GOME measurements: a signature of anthropogenic sources, Atmos. Chem. Phys., 3, 2225–2232, https://doi.org/10.5194/acp-3-2225-2003, 2003.

Boersma, K. F., Eskes, H. J., and Brinksma, E. J.: Error analysis for tropospheric NO_2 retrieval from space: ERROR ANALYSIS FOR TROPOSPHERIC NO_2, J. Geophys. Res., 109, n/a-n/a, https://doi.org/10.1029/2003JD003962, 2004.

Boersma, K. F., Eskes, H. J., Veefkind, J. P., Brinksma, E. J., van der A, R. J., Sneep, M., van den Oord, G. H. J., Levelt, P. F., Stammes, P., Gleason, J. F., and Bucsela, E. J.: Near-real time retrieval of tropospheric NO_2 from OMI, Atmos. Chem. Phys., 7, 2103–2118, https://doi.org/10.5194/acp-7-2103-2007, 2007.

Boersma, K. F., Eskes, H. J., Richter, A., De Smedt, I., Lorente, A., Beirle, S., van Geffen, J. H. G. M., Zara, M., Peters, E., Van Roozendael, M., Wagner, T., Maasakkers, J. D., van der A, R. J., Nightingale, J., De Rudder, A., Irie, H., Pinardi, G., Lambert, J.-C., and Compernolle, S. C.: Improving algorithms and uncertainty estimates for satellite NO_2 retrievals: results from the quality assurance for the essential climate variables (QA4ECV) project, Atmos. Meas. Tech., 11, 6651–6678, https://doi.org/10.5194/amt-11-6651-2018, 2018.

Brauer, M., Hoek, G., Van Vliet, P., Meliefste, K., Fischer, P. H., Wijga, A., Koopman, L. P., Neijens, H. J., Gerritsen, J., Kerkhof, M., Heinrich, J., Bellander, T., and Brunekreef, B.: Air Pollution from Traffic and the Development of Respiratory

https://doi.org/10.5194/amt-2022-51
Preprint. Discussion started: 17 February 2022

Infections and Asthmatic and Allergic Symptoms in Children, Am J Respir Crit Care Med, 166, 1092–1098, https://doi.org/10.1164/rccm.200108-007OC, 2002.

Burrows, J. P., Hölzle, E., Goede, A. P. H., Visser, H., and Fricke, W.: SCIAMACHY—scanning imaging absorption spectrometer for atmospheric chartography, Acta Astronautica, 35, 445–451, https://doi.org/10.1016/0094-5765(94)00278-T, 1995.

Burrows, J. P., Weber, M., Buchwitz, M., Rozanov, V., Ladstätter-Weißenmayer, A., Richter, A., DeBeek, R., Hoogen, R., Bramstedt, K., Eichmann, K.-U., Eisinger, M., and Perner, D.: The Global Ozone Monitoring Experiment (GOME): Mission Concept and First Scientific Results, 56, 151–175, https://doi.org/10.1175/1520-0469(1999)056<0151:TGOMEG>2.0.CO;2, 1999.

BYUN, D.: Science algorithms of the EPA Models-3 Community Multiscale Air Quality (CMAQ) Modeling System, 1999.

Byun, D. and Schere, K. L.: Review of the Governing Equations, Computational Algorithms, and Other Components of the Models-3 Community Multiscale Air Quality (CMAQ) Modeling System, Appl. Mech. Rev., 59, 51, https://doi.org/10.1115/1.2128636, 2006.

Callies, J., Corpaccioli, E., Eisinger, M., Hahne, A., and Lefebvre, A.: GOME-2-Metop's second-generation sensor for operational ozone monitoring, ESA Bull, 1, 28–36, 2000.

Castellanos, P., Boersma, K. F., Torres, O., and de Haan, J. F.: OMI tropospheric NO_2 air mass factors over South America: effects of biomass burning aerosols, Atmos. Meas. Tech., 8, 3831–3849, https://doi.org/10.5194/amt-8-3831-2015, 2015.

Chance, K. and Kurucz, R. L.: An improved high-resolution solar reference spectrum for earth's atmosphere measurements in the ultraviolet, visible, and near infrared, Journal of Quantitative Spectroscopy and Radiative Transfer, 111, 1289–1295, https://doi.org/10.1016/j.jqsrt.2010.01.036, 2010.

Chance, K. V. and Spurr, R. J. D.: Ring effect studies: Rayleigh scattering, including molecular parameters for rotational Raman scattering, and the Fraunhofer spectrum, Appl. Opt., 36, 5224, https://doi.org/10.1364/AO.36.005224, 1997.

Choi, S., Lamsal, L. N., Follette-Cook, M., Joiner, J., Krotkov, N. A., Swartz, W. H., Pickering, K. E., Loughner, C. P., Appel, W., Pfister, G., Saide, P. E., Cohen, R. C., Weinheimer, A. J., and Herman, J. R.: Assessment of NO_2 observations during DISCOVER-AQ and KORUS-AQ field campaigns, Atmos. Meas. Tech., 13, 2523–2546, https://doi.org/10.5194/amt-13-2523-2020, 2020.

Choi, W. J.: Introducing the geostationary environment monitoring spectrometer, J. Appl. Rem. Sens., 12, 1, https://doi.org/10.1117/1.JRS.12.044005, 2018.

Chong, H., Lee, S., Kim, J., Jeong, U., Li, C., Krotkov, N. A., Nowlan, C. R., Al-Saadi, J. A., Janz, S. J., Kowalewski, M. G., Ahn, M.-H., Kang, M., Joiner, J., Haffner, D. P., Hu, L., Castellanos, P., Huey, L. G., Choi, M., Song, C. H., Han, K. M., and Koo, J.-H.: High-resolution mapping of SO2 using airborne observations from the GeoTASO instrument during the KORUS-AQ field study: PCA-based vertical column retrievals, Remote Sensing of Environment, 241, 111725, https://doi.org/10.1016/j.rse.2020.111725, 2020.

Choo, G.-H., Seo, J., Yoon, J., Kim, D.-R., and Lee, D.-W.: Analysis of long-term (2005–2018) trends in tropospheric NO_2 percentiles over Northeast Asia, Atmospheric Pollution Research, 11, 1429–1440, https://doi.org/10.1016/j.apr.2020.05.012, 2020.

Danckaert, T., Fayt, C., Van Roozendael, M., De Smedt, I., Letocart, V., Merlaud, A., and Pinardi, G.: QDOAS Software user manual, Belgian Institute for Space Aeronomy, 2016.

de Foy, B., Lu, Z., and Streets, D. G.: Satellite NO_2 retrievals suggest China has exceeded its NOx reduction goals from the twelfth Five-Year Plan, Sci Rep, 6, 35912, https://doi.org/10.1038/srep35912, 2016.

van Geffen, J., Boersma, K. F., Eskes, H., Sneep, M., ter Linden, M., Zara, M., and Veefkind, J. P.: S5P TROPOMI NO_2 slant column retrieval: method, stability, uncertainties and comparisons with OMI, Atmos. Meas. Tech., 13, 1315–1335, https://doi.org/10.5194/amt-13-1315-2020, 2020.

Guenther, A., Karl, T., Harley, P., Wiedinmyer, C., Palmer, P. I., and Geron, C.: Estimates of global terrestrial isoprene emissions using MEGAN (Model of Emissions of Gases and Aerosols from Nature), Atmos. Chem. Phys., 6, 3181–3210, https://doi.org/10.5194/acp-6-3181-2006, 2006.

Guenther, A. B., Jiang, X., Heald, C. L., Sakulyanontvittaya, T., Duhl, T., Emmons, L. K., and Wang, X.: The Model of Emissions of Gases and Aerosols from Nature version 2.1 (MEGAN2.1): an extended and updated framework for modeling biogenic emissions, Geosci. Model Dev., 5, 1471–1492, https://doi.org/10.5194/gmd-5-1471-2012, 2012.

Herman, J., Cede, A., Spinei, E., Mount, G., Tzortziou, M., and Abuhassan, N.: NO_2 column amounts from ground-based Pandora and MFDOAS spectrometers using the direct-sun DOAS technique: Intercomparisons and application to OMI validation, J. Geophys. Res., 114, D13307, https://doi.org/10.1029/2009JD011848, 2009.

Herman, J., Spinei, E., Fried, A., Kim, J., Kim, J., Kim, W., Cede, A., Abuhassan, N., and Segal-Rozenhaimer, M.: NO_2 and HCHO measurements in Korea from 2012 to 2016 from Pandora spectrometer instruments compared with OMI retrievals and with aircraft measurements during the KORUS-AQ campaign, Atmos. Meas. Tech., 11, 4583–4603, https://doi.org/10.5194/amt-11-4583-2018, 2018.

Hong, H., Lee, H., Kim, J., Jeong, U., Ryu, J., and Lee, D.: Investigation of Simultaneous Effects of Aerosol Properties and Aerosol Peak Height on the Air Mass Factors for Space-Borne NO_2 Retrievals, Remote Sensing, 9, 208, https://doi.org/10.3390/rs9030208, 2017.

Jeong, U., and H. Hong: Assessment of tropospheric concentrations of NO_2 from the TROPOMI/Sentinel-5 Precursor for the estimation of long-term exposure to surface NO_2 over South Korea, Remote Sensing, 13, 1877, https://doi.org/10.3390/rs13101877, 2021a.

Jeong, U., and H. Hong: Comparison of total column and surface mixing ratio of carbon monoxide derived from the TROPOMI/Sentinel-5 Precursor with In-Situ measurements from extensive ground-based network over South Korea, Remote Sensing, 13, 3987, https://doi.org/10.3390/rs13193987, 2021b.

Judd, L. M., Al-Saadi, J. A., Valin, L. C., Pierce, R. B., Yang, K., Janz, S. J., Kowalewski, M. G., Szykman, J. J., Tiefengraber, M., and Mueller, M.: The Dawn of Geostationary Air Quality Monitoring: Case Studies From Seoul and Los Angeles, Front. Environ. Sci., 6, 85, https://doi.org/10.3389/fenvs.2018.00085, 2018.

Judd, L. M., Al-Saadi, J. A., Janz, S. J., Kowalewski, M. G., Pierce, R. B., Szykman, J. J., Valin, L. C., Swap, R., Cede, A., Mueller, M., Tiefengraber, M., Abuhassan, N., and Williams, D.: Evaluating the impact of spatial resolution on tropospheric NO_2 column comparisons within urban areas using high-resolution airborne data, Atmos. Meas. Tech., 12, 6091–6111, https://doi.org/10.5194/amt-12-6091-2019, 2019.

Judd, L. M., Al-Saadi, J. A., Szykman, J. J., Valin, L. C., Janz, S. J., Kowalewski, M. G., Eskes, H. J., Veefkind, J. P., Cede, A., Mueller, M., Gebetsberger, M., Swap, R., Pierce, R. B., Nowlan, C. R., Abad, G. G., Nehrir, A., and Williams, D.: Evaluating Sentinel-5P TROPOMI tropospheric NO_2 column densities with airborne and Pandora spectrometers near New York City and Long Island Sound, Atmos. Meas. Tech., 13, 6113–6140, https://doi.org/10.5194/amt-13-6113-2020, 2020.

Kendrick, C. M., Koonce, P., and George, L. A.: Diurnal and seasonal variations of NO, NO_2 and $PM_{2.5}$ mass as a function of traffic volumes alongside an urban arterial, Atmospheric Environment, 122, 133–141, https://doi.org/10.1016/j.atmosenv.2015.09.019, 2015.

Kim, D., Lee, H., Hong, H., Choi, W., Lee, Y., and Park, J.: Estimation of Surface NO_2 Volume Mixing Ratio in Four Metropolitan Cities in Korea Using Multiple Regression Models with OMI and AIRS Data, Remote Sensing, 9, 627, https://doi.org/10.3390/rs9060627, 2017.

Kim, J., Jeong, U., Ahn, M.-H., Kim, J. H., Park, R. J., Lee, H., Song, C. H., Choi, Y.-S., Lee, K.-H., Yoo, J.-M., Jeong, M.-J., Park, S. K., Lee, K.-M., Song, C.-K., Kim, S.-W., Kim, Y. J., Kim, S.-W., Kim, M., Go, S., Liu, X., Chance, K., Chan Miller, C., Al-Saadi, J., Veihelmann, B., Bhartia, P. K., Torres, O., Abad, G. G., Haffner, D. P., Ko, D. H., Lee, S. H., Woo, J.-H., Chong, H., Park, S. S., Nicks, D., Choi, W. J., Moon, K.-J., Cho, A., Yoon, J., Kim, S., Hong, H., Lee, K., Lee, H., Lee, S., Choi, M., Veefkind, P., Levelt, P. F., Edwards, D. P., Kang, M., Eo, M., Bak, J., Baek, K., Kwon, H.-A., Yang, J., Park, J., Han, K. M., Kim, B.-R., Shin, H.-W., Choi, H., Lee, E., Chong, J., Cha, Y., Koo, J.-H., Irie, H., Hayashida, S., Kasai, Y., Kanaya, Y., Liu, C., Lin, J., Crawford, J. H., Carmichael, G. R., Newchurch, M. J., Lefer, B. L., Herman, J. R., Swap, R. J., Lau, A. K. H., Kurosu, T. P., Jaross, G., Ahlers, B., Dobber, M., McElroy, C. T., and Choi, Y.: New Era of Air Quality Monitoring from Space: Geostationary Environment Monitoring Spectrometer (GEMS), 101, E1–E22, https://doi.org/10.1175/BAMS-D-18-0013.1, 2020.

Kley, D. and McFarland, M.: Chemiluminescence detector for NO and NO_2, Atmos. Technol.; (United States), 12, 1980.

Kowalewski, M. G. and Janz, S. J.: Remote sensing capabilities of the GEO-CAPE airborne simulator, SPIE Optical Engineering + Applications, San Diego, California, United States, 92181I, https://doi.org/10.1117/12.2062058, 2014.

Kowalewski, M.G., Janz, S., Al-Saadi, J.A., Good, W., Ruppert, L., Cole, J.: GeoTASO instrument characterization and level1b radiance product generation, In: Proceedings of the 1st KORUS-AQ Science Team Meeting, Jeju, South Korea, 27 February–3 March 2017, 13. 2017

https://doi.org/10.5194/amt-2022-51
Preprint. Discussion started: 17 February 2022

Atmospheric Measurement Techniques Discussions

Lamsal, L. N., Martin, R. V., Parrish, D. D., and Krotkov, N. A.: Scaling Relationship for NO_2 Pollution and Urban Population Size: A Satellite Perspective, Environ. Sci. Technol., 47, 7855–7861, https://doi.org/10.1021/es400744g, 2013.

Lamsal, L. N., Janz, S. J., Krotkov, N. A., Pickering, K. E., Spurr, R. J. D., Kowalewski, M. G., Loughner, C. P., Crawford, J. H., Swartz, W. H., and Herman, J. R.: High-resolution NO_2 observations from the Airborne Compact Atmospheric Mapper: Retrieval and validation, J. Geophys. Res. Atmos., 122, 1953–1970, https://doi.org/10.1002/2016JD025483, 2017.

Latza, U., Gerdes, S., and Baur, X.: Effects of nitrogen dioxide on human health: Systematic review of experimental and epidemiological studies conducted between 2002 and 2006, International Journal of Hygiene and Environmental Health, 212, 271–287, https://doi.org/10.1016/j.ijheh.2008.06.003, 2009.

Lee, K., Yu, J., Lee, S., Park, M., Hong, H., Park, S. Y., Choi, M., Kim, J., Kim, Y., Woo, J.-H., Kim, S.-W., and Song, C. H.: Development of Korean Air Quality Prediction System version 1 (KAQPS v1) with focuses on practical issues, Geosci. Model Dev., 13, 1055–1073, https://doi.org/10.5194/gmd-13-1055-2020, 2020.

Leitão, J., Richter, A., Vrekoussis, M., Kokhanovsky, A., Zhang, Q. J., Beekmann, M., and Burrows, J. P.: On the improvement of NO_2 satellite retrievals–aerosol impact on the airmass factors, Atmos. Meas. Tech., 3, 475–493, https://doi.org/10.5194/amt-3-475-2010, 2010.

Leitch, J. W., Delker, T., Good, W., Ruppert, L., Murcray, F., Chance, K., Liu, X., Nowlan, C., Janz, S. J., Krotkov, N. A., Pickering, K. E., Kowalewski, M., and Wang, J.: The GeoTASO airborne spectrometer project, SPIE Optical Engineering + Applications, San Diego, California, United States, 92181H, https://doi.org/10.1117/12.2063763, 2014.

Levelt, P. F., van den Oord, G. H. J., Dobber, M. R., Malkki, A., Huib Visser, Johan de Vries, Stammes, P., Lundell, J. O. V., and Saari, H.: The ozone monitoring instrument, IEEE Trans. Geosci. Remote Sensing, 44, 1093–1101, https://doi.org/10.1109/TGRS.2006.872333, 2006.

Lorente, A., Folkert Boersma, K., Yu, H., Dörner, S., Hilboll, A., Richter, A., Liu, M., Lamsal, L. N., Barkley, M., De Smedt, I., Van Roozendael, M., Wang, Y., Wagner, T., Beirle, S., Lin, J.-T., Krotkov, N., Stammes, P., Wang, P., Eskes, H. J., and Krol, M.: Structural uncertainty in air mass factor calculation for NO_2 and HCHO satellite retrievals, Atmos. Meas. Tech., 10, 759–782, https://doi.org/10.5194/amt-10-759-2017, 2017.

Ma, J. Z., Beirle, S., Jin, J. L., Shaiganfar, R., Yan, P., and Wagner, T.: Tropospheric NO_2 vertical column densities over Beijing: results of the first three years of ground-based MAX-DOAS measurements (2008–2011) and satellite validation, Atmos. Chem. Phys., 13, 1547–1567, https://doi.org/10.5194/acp-13-1547-2013, 2013.

Merlaud, A., Constantin, D., Mingireanu, F., Mocanu, I., Maes, J., Fayt, C., Voiculescu, M., Murariu, G., Georgescu, L., Van Roozendael, M.: Small whiskbroom imager for atmospheric composition monitoring (SWING) from an unmanned aerial vehicle (UAV), in: Proceedings of the 21st ESA Symposium on European Rocket & Balloon Programmes and related Research, Thun, Switzerland pp.9–13, 2013.

Meier, A. C., Schönhardt, A., Bösch, T., Richter, A., Seyler, A., Ruhtz, T., Constantin, D.-E., Shaiganfar, R., Wagner, T., Merlaud, A., Van Roozendael, M., Belegante, L., Nicolae, D., Georgescu, L., and Burrows, J. P.: High-resolution airborne imaging DOAS measurements of NO_2 above Bucharest during AROMAT, Atmos. Meas. Tech., 10, 1831–1857, https://doi.org/10.5194/amt-10-1831-2017, 2017.

Merlaud, A., Tack, F., Constantin, D., Georgescu, L., Maes, J., Fayt, C., Mingireanu, F., Schuettemeyer, D., Meier, A. C., Schönardt, A., Ruhtz, T., Bellegante, L., Nicolae, D., Den Hoed, M., Allaart, M., and Van Roozendael, M.: The Small Whiskbroom Imager for atmospheric compositioN monitorinG (SWING) and its operations from an unmanned aerial vehicle (UAV) during the AROMAT campaign, Atmos. Meas. Tech., 11, 551–567, https://doi.org/10.5194/amt-11-551-2018, 2018.

Nowlan, C. R., Liu, X., Leitch, J. W., Chance, K., González Abad, G., Liu, C., Zoogman, P., Cole, J., Delker, T., Good, W., Murcray, F., Ruppert, L., Soo, D., Follette-Cook, M. B., Janz, S. J., Kowalewski, M. G., Loughner, C. P., Pickering, K. E., Herman, J. R., Beaver, M. R., Long, R. W., Szykman, J. J., Judd, L. M., Kelley, P., Luke, W. T., Ren, X., and Al-Saadi, J. A.: Nitrogen dioxide observations from the Geostationary Trace gas and Aerosol Sensor Optimization (GeoTASO) airborne instrument: Retrieval algorithm and measurements during DISCOVER-AQ Texas 2013, Atmos. Meas. Tech., 9, 2647–2668, https://doi.org/10.5194/amt-9-2647-2016, 2016.

Nowlan, C. R., Liu, X., Leitch, J. W., Chance, K., A., González Abad, Liu, C., Zoogman, P., Cole, J., Delker, T., Good, W., Murcray, F., Ruppert, L., Soo, D., Follette-Cook, M. B., Janz, S. J., Kowalewski, M. G., Loughner, C. P., Pickering,K. E., Herman, J. R., Beaver, M. R., Long, R. W., Szykman, J. J., Judd, L. M., Kelley, P., Luke, W. T., Ren, W., and Sl-Saadi, J. A.: Nitrogen dioxide observations from the Geostationary Trace gas and Aerosol Sensor Optimization (GeoTASO) airborne instrument: Retrieval algorithm and measurements during DISCOVER-AQ Texas 2013, Atmos. Meas. Tech., 9, 2647-2668, http://doi.org/10.5194/atm-9-2647-2016, 2016.

Nowlan, C. R., Liu, X., Janz, S. J., Kowalewski, M. G., Chance, K., Follette-Cook, M. B., Fried, A., González Abad, G., Herman, J. R., Judd, L. M., Kwon, H.-A., Loughner, C. P., Pickering, K. E., Richter, D., Spinei, E., Walega, J., Weibring, P., and Weinheimer, A. J.: Nitrogen dioxide and formaldehyde measurements from the GEOstationary Coastal and Air Pollution Events (GEO-CAPE) Airborne Simulator over Houston, Texas, Atmos. Meas. Tech., 11, 5941–5964, https://doi.org/10.5194/amt-11-5941-2018, 2018.

Palmer, P. I., Jacob, D. J., Chance, K., Martin, R. V., Spurr, R. J. D., Kurosu, T. P., Bey, I., Yantosca, R., Fiore, A., and Li, Q.: Air mass factor formulation for spectroscopic measurements from satellites: Application to formaldehyde retrievals from the Global Ozone Monitoring Experiment, J. Geophys. Res., 106, 14539–14550, https://doi.org/10.1029/2000JD900772, 2001.

Pastel, M., Pommereau, J.-P., Goutail, F., Richter, A., Pazmiño, A., Ionov, D., and Portafaix, T.: Construction of merged satellite total O_3 and NO_2 time series in the tropics for trend studies and evaluation by comparison to NDACC SAOZ measurements, Atmos. Meas. Tech., 7, 3337–3354, https://doi.org/10.5194/amt-7-3337-2014, 2014.

Platt, U.: Differential absorption spectroscopy (DOAS), Chem. Anal. Series, 127, 27–83, 1994.

Platt, U., Stutz, J.: Differential absorption spectroscopy, in: Differential Optical Absorption Spectroscopy, Springer, Berlin, Heidelberg, pp. 135–174, 2008.

Popp, C., Brunner, D., Damm, A., Van Roozendael, M., Fayt, C., and Buchmann, B.: High-resolution NO_2 remote sensing from the Airborne Prism EXperiment (APEX) imaging spectrometer, Atmos. Meas. Tech., 5, 2211–2225, https://doi.org/10.5194/amt-5-2211-2012, 2012.

Prasad, A. K., Singh, R. P., and Kafatos, M.: Influence of coal-based thermal power plants on the spatial–temporal variability of tropospheric NO_2 column over India, Environ Monit Assess, 184, 1891–1907, https://doi.org/10.1007/s10661-011-2087-6, 2012.

Qin, K., Rao, L., Xu, J., Bai, Y., Zou, J., Hao, N., Li, S., and Yu, C.: Estimating Ground Level NO_2 Concentrations over Central-Eastern China Using a Satellite-Based Geographically and Temporally Weighted Regression Model, Remote Sensing, 9, 950, https://doi.org/10.3390/rs9090950, 2017.

Richter, A. and Burrows, J. P.: Tropospheric NO_2 from GOME measurements, Advances in Space Research, 29, 1673–1683, https://doi.org/10.1016/S0273-1177(02)00100-X, 2002.

Richter, A., Burrows, J. P., Nüß, H., Granier, C., and Niemeier, U.: Increase in tropospheric nitrogen dioxide over China observed from space, Nature, 437, 129–132, https://doi.org/10.1038/nature04092, 2005.

Richter, A., Begoin, M., Hilboll, A., and Burrows, J. P.: An improved NO_2 retrieval for the GOME-2 satellite instrument, Atmos. Meas. Tech., 4, 1147–1159, https://doi.org/10.5194/amt-4-1147-2011, 2011.

Schönhardt, A., Altube, P., Gerilowski, K., Krautwurst, S., Hartmann, J., Meier, A. C., Richter, A., and Burrows, J. P.: A wide field-of-view imaging DOAS instrument for two-dimensional trace gas mapping from aircraft, Atmos. Meas. Tech., 8, 5113–5131, https://doi.org/10.5194/amt-8-5113-2015, 2015.

Shah, V., Jacob, D. J., Li, K., Silvern, R. F., Zhai, S., Liu, M., Lin, J., and Zhang, Q.: Effect of changing NO_x lifetime on the seasonality and long-term trends of satellite-observed tropospheric NO_2 columns over China, Atmos. Chem. Phys., 20, 1483–1495, https://doi.org/10.5194/acp-20-1483-2020, 2020.

Sioris, C. E., Kurosu, T. P., Martin, R. V., and Chance, K.: Stratospheric and tropospheric NO_2 observed by SCIAMACHY: first results, Advances in Space Research, 34, 780–785, https://doi.org/10.1016/j.asr.2003.08.066, 2004.

Skamarock, W., Klemp, J., Dudhia, J., Gill, D., Barker, D., Wang, W., Huang, X.-Y., and Duda, M.: A Description of the Advanced Research WRF Version 3, UCAR/NCAR, https://doi.org/10.5065/D68S4MVH, 2008.

Spinei, E., Whitehill, A., Fried, A., Tiefengraber, M., Knepp, T. N., Herndon, S., Herman, J. R., Müller, M., Abuhassan, N., Cede, A., Richter, D., Walega, J., Crawford, J., Szykman, J., Valin, L., Williams, D. J., Long, R., Swap, R. J., Lee, Y., Nowak, N., and Poche, B.: The first evaluation of formaldehyde column observations by improved Pandora spectrometers during the KORUS-AQ field study, Atmos. Meas. Tech., 11, 4943–4961, https://doi.org/10.5194/amt-11-4943-2018, 2018.

Spurr, R. and Christi, M.: On the generation of atmospheric property Jacobians from the (V)LIDORT linearized radiative transfer models, Journal of Quantitative Spectroscopy and Radiative Transfer, 142, 109–115, https://doi.org/10.1016/j.jqsrt.2014.03.011, 2014.

https://doi.org/10.5194/amt-2022-51
Preprint. Discussion started: 17 February 2022

Tack, F., Merlaud, A., Iordache, M.-D., Danckaert, T., Yu, H., Fayt, C., Meuleman, K., Deutsch, F., Fierens, F., and Van Roozendael, M.: High-resolution mapping of the NO_2 spatial distribution over Belgian urban areas based on airborne APEX remote sensing, Atmos. Meas. Tech., 10, 1665–1688, https://doi.org/10.5194/amt-10-1665-2017, 2017.

Tack, F., Merlaud, A., Meier, A. C., Vlemmix, T., Ruhtz, T., Iordache, M.-D., Ge, X., van der Wal, L., Schuettemeyer, D., Ardelean, M., Calcan, A., Constantin, D., Schönhardt, A., Meuleman, K., Richter, A., and Van Roozendael, M.: Intercomparison of four airborne imaging DOAS systems for tropospheric NO_2 mapping–the AROMAPEX campaign, Atmos. Meas. Tech., 12, 211–236, https://doi.org/10.5194/amt-12-211-2019, 2019.

Tack, F., Merlaud, A., Iordache, M.-D., Pinardi, G., Dimitropoulou, E., Eskes, H., Bomans, B., Veefkind, P., and Van Roozendael, M.: Assessment of the TROPOMI tropospheric NO_2 product based on airborne APEX observations, Atmos. Meas. Tech., 14, 615–646, https://doi.org/10.5194/amt-14-615-2021, 2021.

Tzortziou, M., Parker, O., Lamb, B., Herman, J., Lamsal, L., Stauffer, R., and Abuhassan, N.: Atmospheric Trace Gas (NO_2 and O_3) Variability in South Korean Coastal Waters, and Implications for Remote Sensing of Coastal Ocean Color Dynamics, Remote Sensing, 10, 1587, https://doi.org/10.3390/rs10101587, 2018.

Valks, P., Pinardi, G., Richter, A., Lambert, J.-C., Hao, N., Loyola, D., Van Roozendael, M., and Emmadi, S.: Operational total and tropospheric NO_2 column retrieval for GOME-2, Atmos. Meas. Tech., 4, 1491–1514, https://doi.org/10.5194/amt-4-1491-2011, 2011.

Vandaele, A. C., Hermans, C., Simon, P. C., Carleer, M., Colin, R., Fally, S., Mérienne, M. F., Jenouvrier, A., and Coquart, B.: Measurements of the NO_2 absorption cross-section from 42 000 cm^{-1} to 10 000 cm^{-1} (238–1000 nm) at 220 K and 294 K, Journal of Quantitative Spectroscopy and Radiative Transfer, 59, 171–184, https://doi.org/10.1016/S0022-4073(97)00168-4, 1998.

Veefkind, J. P., Aben, I., McMullan, K., Förster, H., de Vries, J., Otter, G., Claas, J., Eskes, H. J., de Haan, J. F., Kleipool, Q., van Weele, M., Hasekamp, O., Hoogeveen, R., Landgraf, J., Snel, R., Tol, P., Ingmann, P., Voors, R., Kruizinga, B., Vink, R., Visser, H., and Levelt, P. F.: TROPOMI on the ESA Sentinel-5 Precursor: A GMES mission for global observations of the atmospheric composition for climate, air quality and ozone layer applications, Remote Sensing of Environment, 120, 70–83, https://doi.org/10.1016/j.rse.2011.09.027, 2012.

Vlemmix, T., Ge, X., de Goeij, B. T. G., van der Wal, L. F., Otter, G. C. J., Stammes, P., Wang, P., Merlaud, A., Schüttemeyer, D., Meier, A. C., Veefkind, J. P., and Levelt, P. F.: Retrieval of tropospheric NO_2 columns over Berlin from high-resolution airborne observations with the spectrolite breadboard instrument, Atmos. Meas. Tech. Discuss., https://doi.org/10.5194/amt-2017-257, in review, 2017.

Wiedinmyer, C., Quayle, B., Geron, C., Belote, A., McKenzie, D., Zhang, X., O'Neill, S., and Wynne, K. K.: Estimating emissions from fires in North America for air quality modeling, Atmospheric Environment, 40, 3419–3432, https://doi.org/10.1016/j.atmosenv.2006.02.010, 2006.

https://doi.org/10.5194/amt-2022-51
Preprint. Discussion started: 17 February 2022

Wiedinmyer, C., Akagi, S. K., Yokelson, R. J., Emmons, L. K., Al-Saadi, J. A., Orlando, J. J., and Soja, A. J.: The Fire INventory from NCAR (FINN): a high resolution global model to estimate the emissions from open burning, Geosci. Model Dev., 4, 625–641, https://doi.org/10.5194/gmd-4-625-2011, 2011.

Wold, S., Esbensen, K., and Geladi, P.: Principal component analysis, Chemometrics and Intelligent Laboratory Systems, 2, 37–52, https://doi.org/10.1016/0169-7439(87)80084-9, 1987.

Woo, J.-H., Choi, K.-C., Kim, H. K., Baek, B. H., Jang, M., Eum, J.-H., Song, C. H., Ma, Y.-I., Sunwoo, Y., Chang, L.-S., and Yoo, S. H.: Development of an anthropogenic emissions processing system for Asia using SMOKE, Atmospheric Environment, 58, 5–13, https://doi.org/10.1016/j.atmosenv.2011.10.042, 2012.

Zoogman, P., Liu, X., Suleiman, R. M., Pennington, W. F., Flittner, D. E., Al-Saadi, J. A., Hilton, B. B., Nicks, D. K., Newchurch, M. J., Carr, J. L., Janz, S. J., Andraschko, M. R., Arola, A., Baker, B. D., Canova, B. P., Chan Miller, C., Cohen, R. C., Davis, J. E., Dussault, M. E., Edwards, D. P., Fishman, J., Ghulam, A., González Abad, G., Grutter, M., Herman, J. R., Houck, J., Jacob, D. J., Joiner, J., Kerridge, B. J., Kim, J., Krotkov, N. A., Lamsal, L., Li, C., Lindfors, A., Martin, R. V., McElroy, C. T., McLinden, C., Natraj, V., Neil, D. O., Nowlan, C. R., O′Sullivan, E. J., Palmer, P. I., Pierce, R. B., Pippin, M. R., Saiz-Lopez, A., Spurr, R. J. D., Szykman, J. J., Torres, O., Veefkind, J. P., Veihelmann, B., Wang, H., Wang, J., and Chance, K.: Tropospheric emissions: Monitoring of pollution (TEMPO), Journal of Quantitative Spectroscopy and Radiative Transfer, 186, 17–39, https://doi.org/10.1016/j.jqsrt.2016.05.008, 2017.

https://doi.org/10.5194/amt-2022-51
Preprint. Discussion started: 17 February 2022

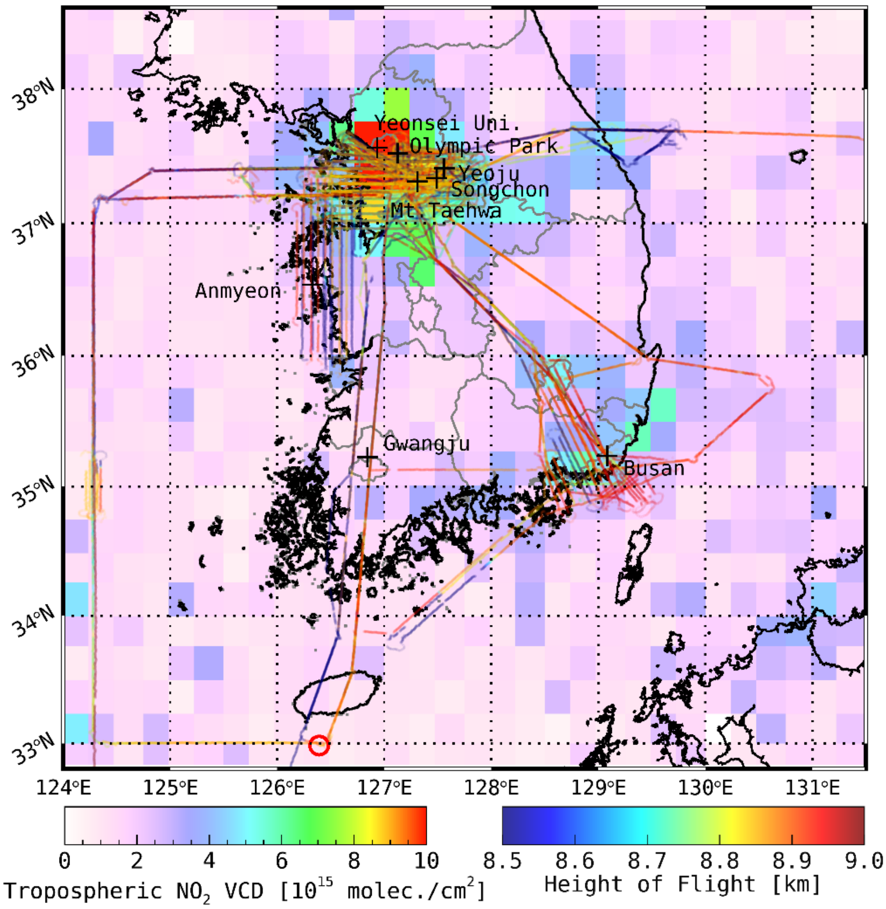

Figure 1. Flight paths of the NASA LaRC B200 aircraft carrying GeoTASO and the average tropospheric NO_2 VCDs obtained from OMI binned to a 0.1°×0.1° horizontal grid during the KORUS-AQ campaign period. The line colour represents flight height. In this period, the GeoTASO observations focused on megacities (Seoul and Busan) and industrial complex area (Anmyeon) with high tropospheric NO_2 concentrations. The reference spectrum for spectral fitting is obtained from the radiation data under the Jeju Island (marked with red circle).

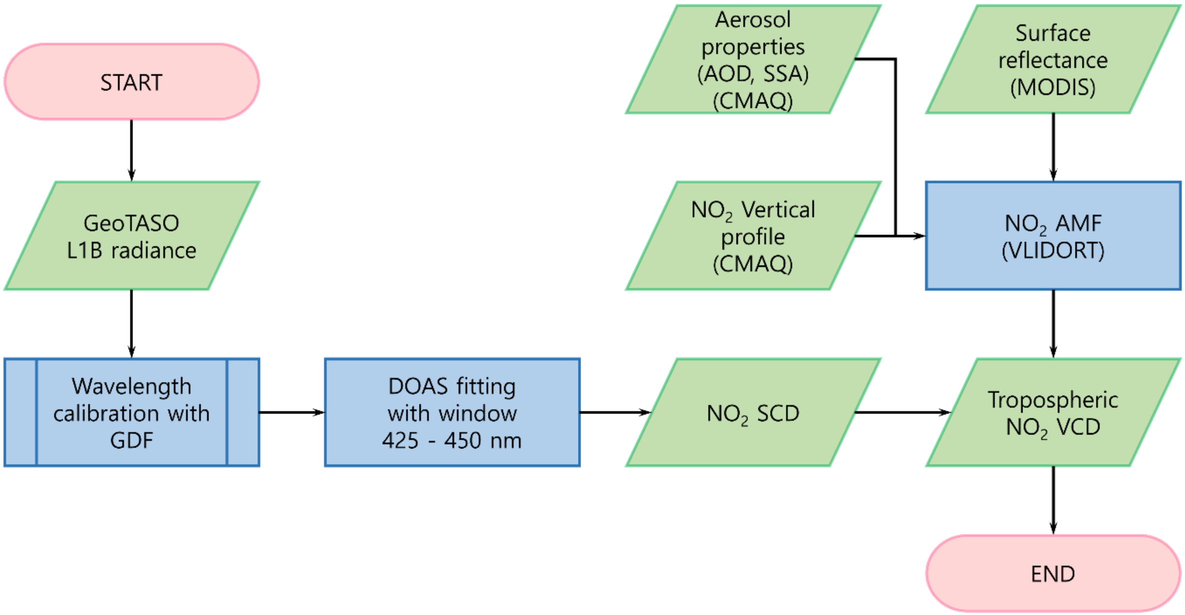

Figure 2. Flowchart of the algorithm for retrieving tropospheric NO_2 data from GeoTASO.

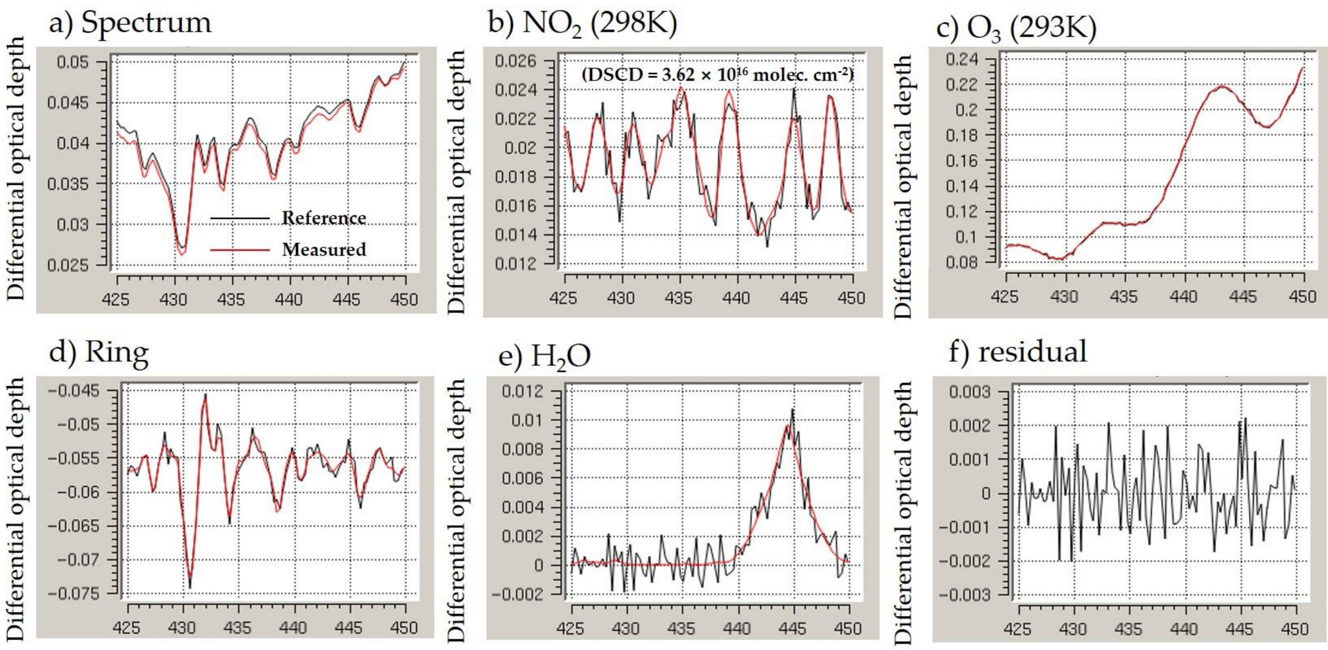

Figure 3. An example of the spectral fitting results of NO_2 retrievals from GeoTASO during the KORUS-AQ campaign (at Gangnam, Seoul on 22 May, 2016). Red and black line in the panel (a) represent measured and reference spectrum, respectively. The panels from (b) to (e) depict examples of spectral fitting results of (b) NO_2, (c) O_3, (d) Ring, and (e) H_2O, where red and black lines are absorption cross section of target species and the fitting residual plus the absorption of the target species, respectively. The panel (f) shows fitting residual of this example

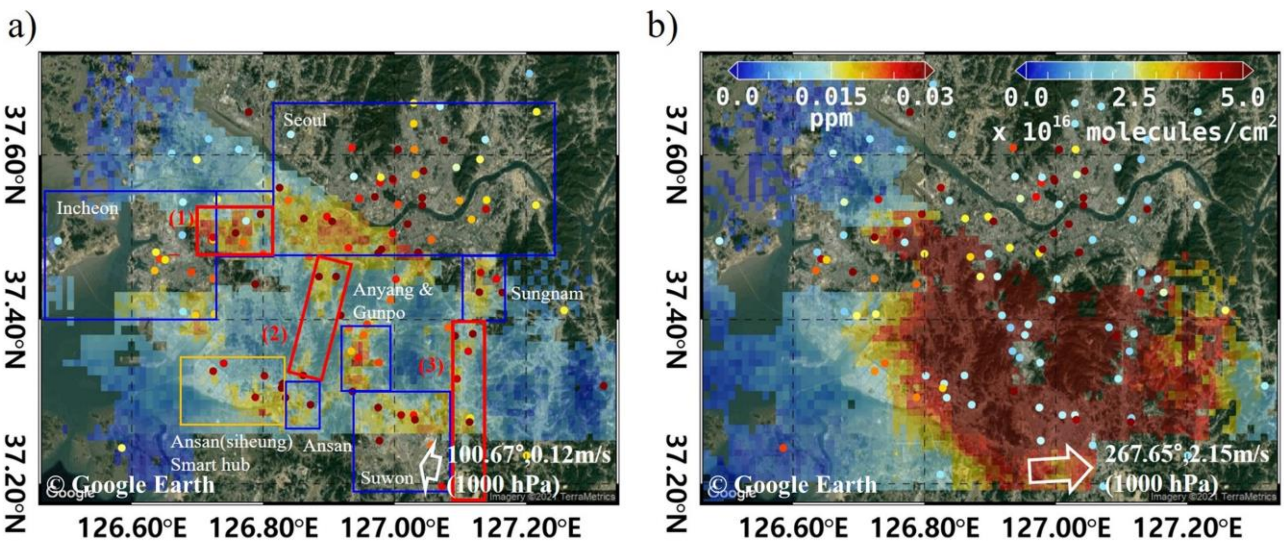

Figure 4. Tropospheric NO_2 VCD, binned to a 0.01°×0.01° horizontal grid, in the Seoul metropolitan region on 9, June 2016 retrieved from GeoTASO: a) at 9 AM and b) at 3 PM. The red boxes represent expressways (counterclockwise from left to right, (1) Gyeongin expressway, (2) Seohaean expressway, and (3) Gyeongbu expressway), the orange box indicates the industrial complex, and the blue boxes indicate the major cities (Seoul, Incheon, Suwon, Bucheon, Anyang, Gunpo, Sungnam, and Ansan) of the Seoul metropolitan region. Colours of the circles depict the NO_2 surface mixing ratio obtained from Air-Korea. The white arrows at the bottom right of the each panel show the wind direction and speed over Anyang, obtained via Unified Model (UM) simulations (background RGB image is from Google Earth; https://www.google.com/maps/).

https://doi.org/10.5194/amt-2022-51
Preprint. Discussion started: 17 February 2022

Atmospheric Measurement Techniques Discussions

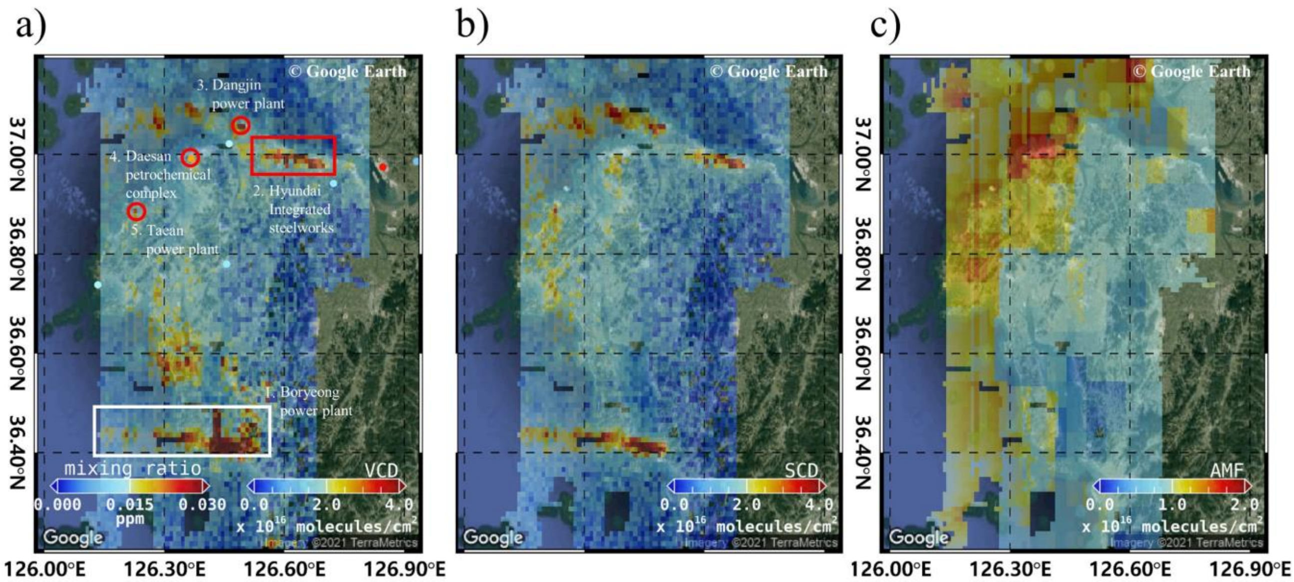

Figure 5. a) Tropospheric NO_2 VCD and b) NO_2 SCD retrieved from GeoTASO, and c) NO_2 AMF calculated using VLIDORT over Anmyeon in South Korea on 5 June 2016. The data were gridded into to a spatial resolution of 0.01°×0.01°. The red circles and rectangle in panel (a) represent the major NO_2 emission sources, such as steelworks and power plants (background RGB image is from Google Earth; https://www.google.com/maps/).

https://doi.org/10.5194/amt-2022-51
Preprint. Discussion started: 17 February 2022

Atmospheric Measurement Techniques Discussions

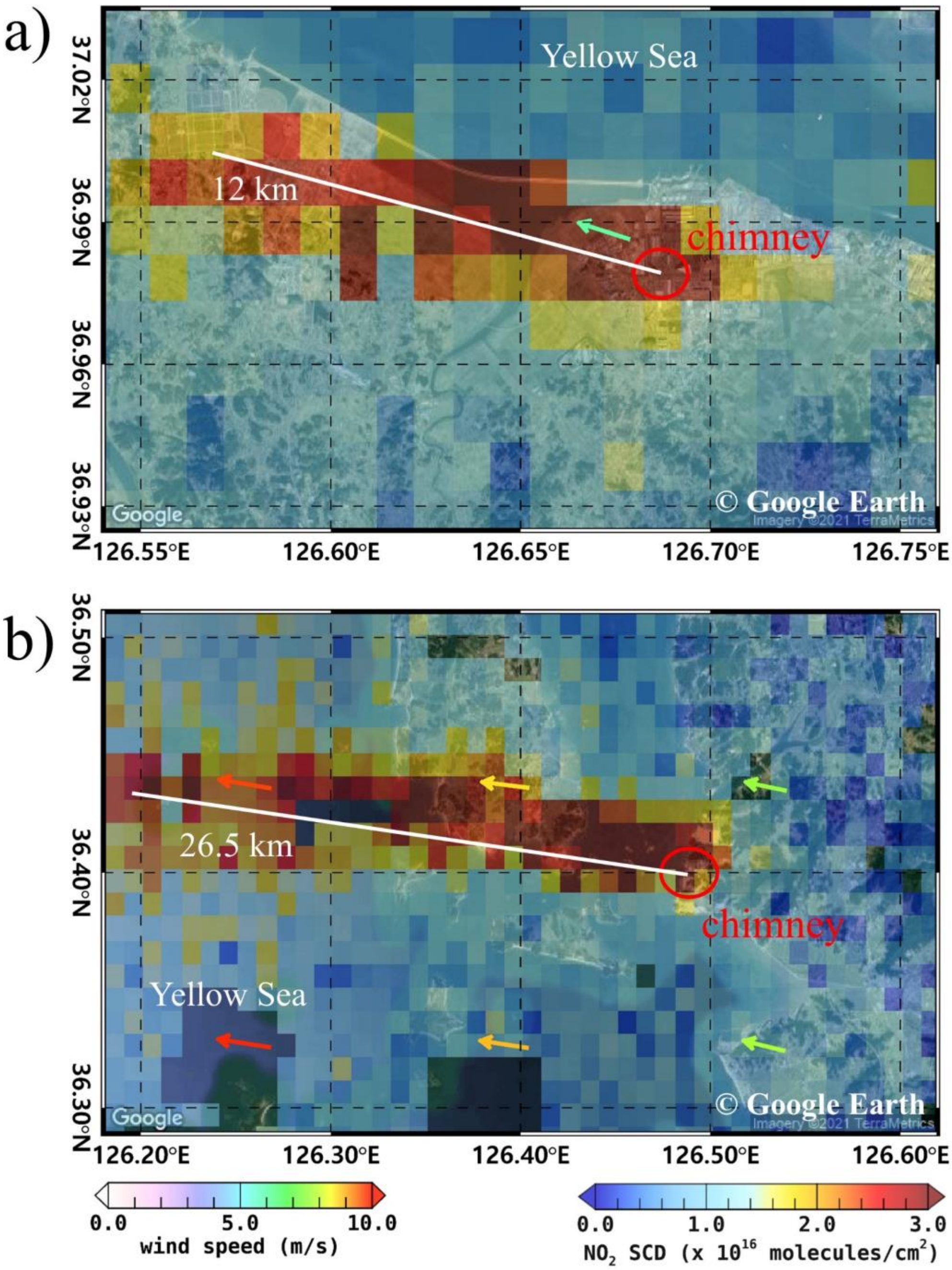

Figure 6. Enlarged view of GeoTASO tropospheric NO_2 VCD observation over a) Hyundai steel works, indicated by the red box in Figure 5, and b) the Boryeong power plant, indicated by the white box in Figure 5. The data were gridded into to a spatial resolution of 0.01°×0.01°. The arrows represent the wind direction and speed (background RGB image is from Google Earth; https://www.google.com/maps/).

https://doi.org/10.5194/amt-2022-51
Preprint. Discussion started: 17 February 2022

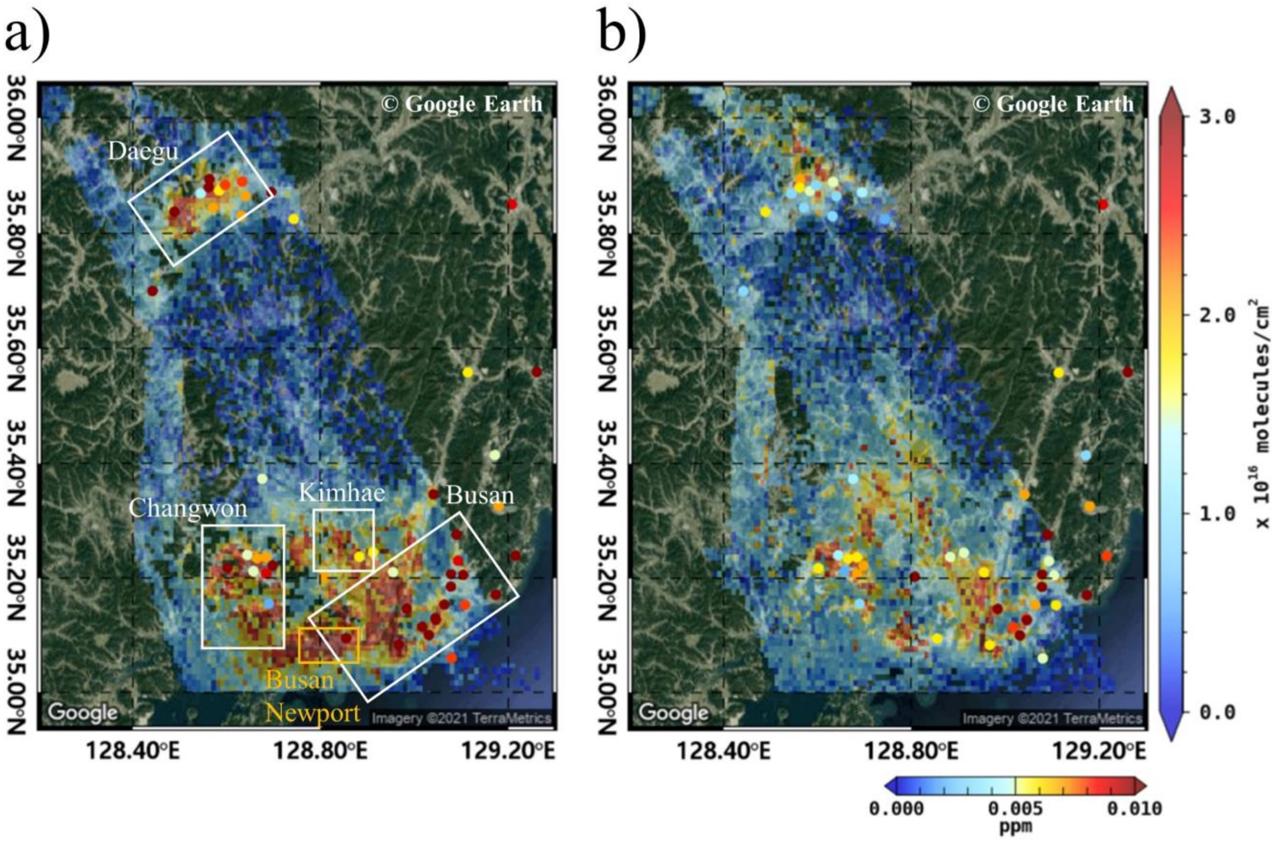

Figure 7. Tropospheric NO_2 VCD in the Busan metropolitan region in the (a) morning and (b) afternoon of 10 June 2016. The data were gridded into to a spatial resolution of 0.01°×0.01°. The white boxes represent major cities such as Busan, Daegu, Changwon, and Kimhae. The orange box represents Busan Newport (background RGB image is from Google Earth; https://www.google.com/maps/).

Atmospheric Measurement Techniques
Open Access
Discussions

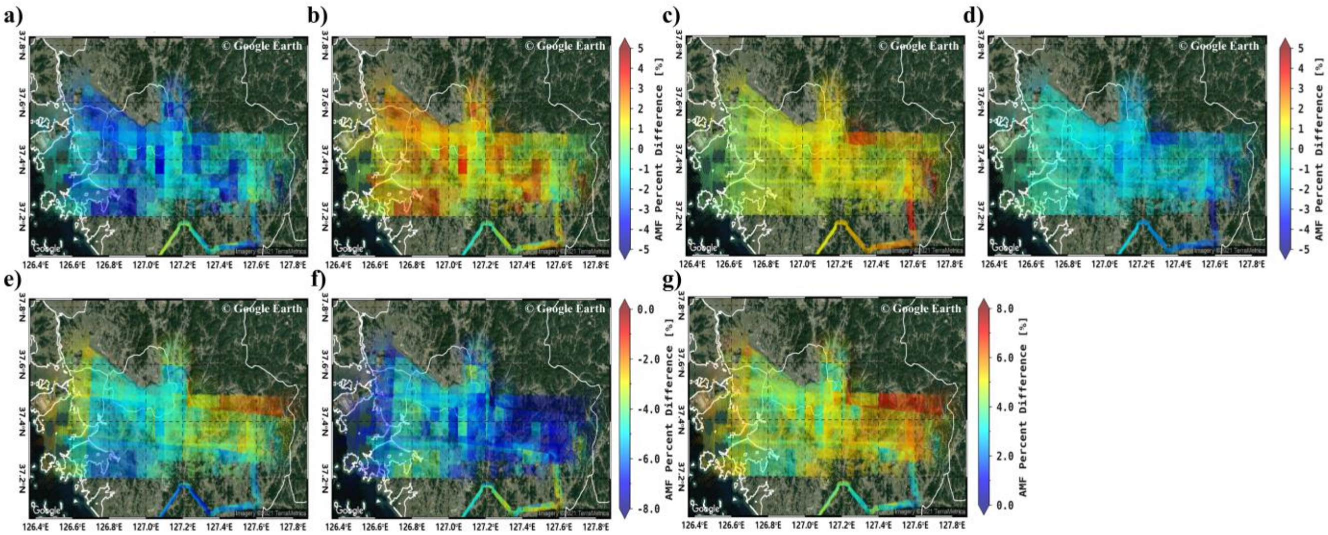

Figure 8. Percentage difference between AMF calculated using the CMAQ model simulation and those using a) 20% lower AOD, b) 20% higher AOD, c) 20% lower aerosol loading height, d) 20% higher aerosol loading height, compared to the model outputs. The percentage difference for AMF calculated using MODIS data and those using e) 4% lower SSA, f) 20% lower surface reflectance, and g) 20% higher surface reflectance (background RGB image is from Google Earth; https://www.google.com/maps/).

https://doi.org/10.5194/amt-2022-51
Preprint. Discussion started: 17 February 2022

Atmospheric Measurement Techniques
Discussions

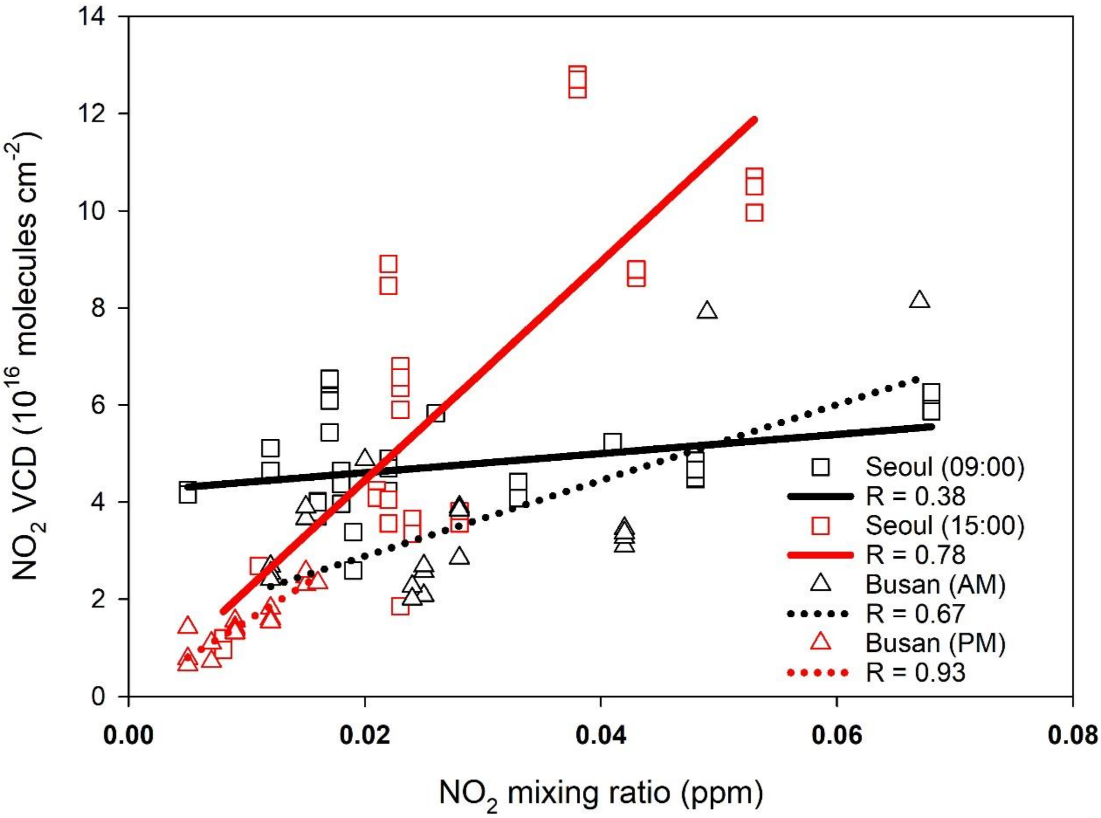

Figure 9. Scatter plot of the NO_2 VCDs retrieved from GeoTASO, and NO_2 surface mixing ratio obtained from Air-Korea. The black and red squares represent the NO_2 data at 9 AM and 3 PM (local time) over the Seoul metropolitan region, respectively. The black and red triangles represent those in the morning and afternoon, over Busan, respectively.

https://doi.org/10.5194/amt-2022-51
Preprint. Discussion started: 17 February 2022

Atmospheric Measurement Techniques Discussions
Open Access

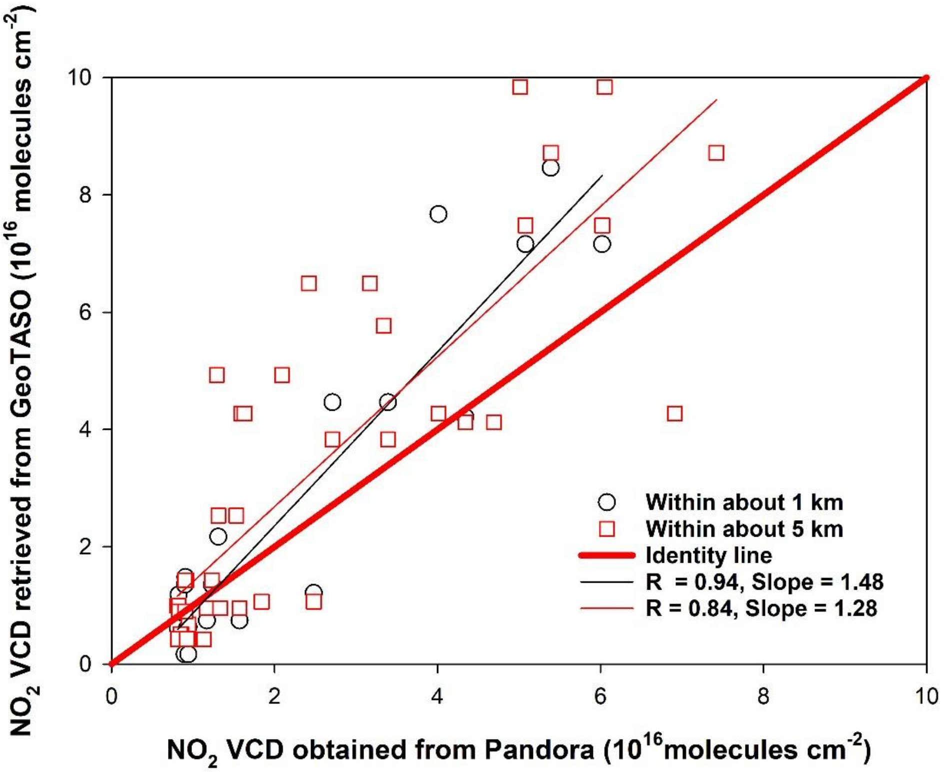

Figure 10. Scatter plot of NO_2 VCDs obtained from Pandora and those retrieved from GeoTASO during Pandora overflight. The black circles and red squares represent the average NO_2 VCD retrieved from GeoTASO within a radius of about 1 km and 5 km from the Pandora site, respectively.

https://doi.org/10.5194/amt-2022-51
Preprint. Discussion started: 17 February 2022

Atmospheric Measurement Techniques
Discussions
Open Access

Table 1. Summary for GeoTASO instrument and optical specification.

L1B version	V02y
Cross-track field of view	45°
Wavelength	UV: 290–400 nm VIS: 415–695 nm
Spectral resolution (full width at half maximum, FWHM)	UV: ~0.39 nm VIS: ~0.88 nm
CCD	1,056 (wavelength) × 1,033 (cross-track)
Spatial resolution before binning	~35 m (along-track) × 7 m (cross-track)
Spatial resolution after binning	~250 m (along-track) × 250 m (cross-track)

https://doi.org/10.5194/amt-2022-51
Preprint. Discussion started: 17 February 2022

Table 2. The population, number of registered vehicles, and average mileage per car of major cities in the Seoul metropolitan region obtained from the Korean Statistical Information Service (kosis.kr/eng).

City	Population (millions)	Vehicle registration number (thousands)	Average mileage per car (km)
Seoul	9.776	3,083	37.1
Incheon	2.914	1,402	41.7
Bucheon	0.848	284	37.2
Ansan	0.744	289	40.8
Anyang	0.596	206	39.6
Gunpo	0.286	87	38.8
Suwon	1.241	467	38.1
Sungnam	0.994	358	36.3

https://doi.org/10.5194/amt-2022-51
Preprint. Discussion started: 17 February 2022

Table 3. Daily average traffic volume on the Gyeongin, Gyeongbu, and Seohaean Expressways obtained using the Traffic Monitoring System (road.re.kr).

Expressway	Daily average traffic volume
Gyeongin Expressway	162,369
Gyeongbu Expressway	173,413
Seohaean Expressway	150,298

https://doi.org/10.5194/amt-2022-51
Preprint. Discussion started: 17 February 2022

Atmospheric Measurement Techniques Discussions
Open Access

Table 4. NO_2 emission rates from major industrial facilities in the Anmyeon region obtained from the Continuous Emission Monitoring System of the Korea Environment Corporation (stacknsky.or.kr/eng/main.html).

Industrial facilities	NO_2 emission rate (2016) (kg/year)
Boryeong power plant	16,788,438
Hyundai integrated steelworks	10,271,075
Dangjin power plant	11,852,972
Daesan petrochemical complex	3,397,939
Taean power plant	15,466,022

https://doi.org/10.5194/amt-2022-51
Preprint. Discussion started: 17 February 2022

Atmospheric Measurement Techniques
Discussions

Table 5. The population, number of registered vehicles, and average mileage per car of major cities in the Busan metropolitan region obtained from the Korean Statistical Information Service (kosis.kr/eng).

City	Population (millions)	Vehicle registration number (thousands)	Average mileage per car (km)
Busan	3.389	1,295	40.1
Daegu	2.450	1,121	37.1
Changwon	1.080	551	37.5
Kimhae	0.529	250	38.0

https://doi.org/10.5194/amt-2022-51
Preprint. Discussion started: 17 February 2022

Atmospheric Measurement Techniques Discussions
Open Access
EGU

Table 6. Total errors of NO_2 VCD caused by uncertainties in NO_2 SCD and NO_2 AMF.

NO_2 AMF errors	AOD	2.0%
	SSA	4.1%
	aerosol loading height	1.0%
	surface reflectance	5.2%
	total NO_2 AMF error due to aerosol uncertainties	**7.3%**
NO_2 SCD error		**11.9%**
NO_2 VCD error		**14.3%**